Applied Catalysis B: Environmental 174–175 (2015) 293–307

Contents lists available at ScienceDirect

Applied Catalysis B: Environmental

journal homepage: www.elsevier.com/locate/apcatb

Active, selective and robust Pd and/or Cr catalysts supported on Ti-, Zr- or [Ti,Zr]-pillared montmorillonites for destruction of chlorinated volatile organic compounds

A. Michalik-Zym[a], R. Dula[a], D. Duraczyńska[a], J. Kryściak-Czerwenka[a], T. Machej[a], R.P. Socha[a], W. Włodarczyk[a,b], A. Gaweł[b], J. Matusik[b], K. Bahranowski[b], E. Wisła-Walsh[c], L. Lityńska-Dobrzyńska[d], E.M. Serwicka[a,*]

[a] Jerzy Haber Institute of Catalysis and Surface Chemistry, Polish Academy of Sciences, Niezapominajek 8, 30-239 Krakow, Poland
[b] AGH University of Science and Technology, Faculty of Geology, Geophysics and Environmental Protection, al. Mickiewicza 30, 30-059 Krakow, Poland
[c] AGH University of Science and Technology, Faculty of Mechanical Engineering and Robotics, al. Mickiewicza 30, 30-059 Krakow, Poland
[d] Institute of Metallurgy and Materials Science, Polish Academy of Sciences, Reymonta 25, 30-059 Krakow, Poland

ARTICLE INFO

Article history:
Received 23 December 2014
Received in revised form 8 March 2015
Accepted 10 March 2015
Available online 12 March 2015

Keywords:
Palladium catalyst
Chromium catalyst
Pillared clay
Chlorinated volatile organic compound
Combustion

ABSTRACT

Pd and/or Cr catalysts supported on Ti-, Zr- or mixed [Ti,Zr]-pillared montomorillonite clays (PILC), for use in combustion of dichloromethane (DCM) and trichloroethylene (TCE), were synthesized, and characterized with XRD, SEM, TEM/HRTEM, XPS, ESR and Raman spectroscopies, N_2 adsorption/desorption at −196 °C, NH_3 TPD–MS, and FTIR of pyridine adsorption. The catalysts are porous solids with high surface area (240–390 m^2/g). Pd exists as fine PdO_x nanoparticles, predominantly of ≤10 nm size, while Cr is present as monomeric CrO_x species. The highest (Pd^{4+} and Cr^{6+}), or next to highest (Cr^{5+}), oxidation states dominate at the catalysts surface. The active phases are most reducible when supported on Ti-PILC and most difficult to reduce on [Ti,Zr]-PILC. Catalysts supported on [Ti,Zr]-PILC show highest total acidity, of predominantly Lewis character. The excellent performance of the catalysts in combustion of DCM and TCE is attributed to the combination of highly porous structure of PILC supports, good dispersion of the active phases, and appropriate blend of redox and acid–base functions. In both reactions, for a given type of support, the catalysts with Cr-only active phase show best performance in terms of activity, which is assigned to the presence of well dispersed, highly oxidized Cr^{6+}/Cr^{5+} species. In DCM combustion, catalysts supported on Ti-PILC show superior activity, attributed to much better reducibility of active phases deposited on this carrier. In TCE oxidation, best activity is obtained for [Ti,Zr]-PILC supported catalysts, which is correlated with the highest Lewis acidity of these samples. Pd-only catalysts are most selective, showing 100% selectivity to HCl and CO_2 at T_{90} for both studied reactions. Cr-only catalysts are least selective, and emit substantial amounts of Cl_2 and CO. Mixed Pd,Cr-catalysts represent an attractive, cheaper alternative to purely Pd systems. At T_{90} their selectivity to CO_2 is 100% in both reactions, with the selectivity to HCl ranging from 87 to 100%. PILC-supported catalyst proved very stable in the reaction environment, both in terms of the catalytic performance and the structural identity.

1. Introduction

Release of chlorinated volatile organics compounds (CVOCs) to the atmosphere accompanies many industrial activities, such as manufacturing of chemicals (e.g., vinyl chloride), degreasing processes, dry cleaning or printing. The compounds are toxic, possess carcinogenic properties, and contribute to the destruction of the ozone layer, hence, their emission constitutes a major environmental hazard [1,2]. Thermal combustion is a conventional, commonly used method of CVOCs removal. However, this technology requires temperatures around 1000 °C, which generates high operating costs [3]. Moreover, high-temperature process leads to the formation of nitrogen oxides and may result in the release of highly toxic dioxins or polychlorinated bifenyls, formed as a result of incomplete combustion of CVOCs [4,5]. Therefore, catalytic oxidation of CVOCs, which can be carried out at temperature below 500 °C, and thus, be free of adverse effects accompanying thermal incineration, is considered a particularly attractive clean-up

* Corresponding author. Tel.: +48 12 6395118; fax: +48 12 4251923.
E-mail address: ncserwic@cyf-kr.edu.pl (E.M. Serwicka).

http://dx.doi.org/10.1016/j.apcatb.2015.03.015
0926-3373/

technology [3,6,7]. Ideally, total oxidation of a CVOC molecule should result in the formation of carbon dioxide, water and hydrogen chloride, the latter being readily scrubbed with a caustic solution downstream of the catalytic reactor. The catalysts reported as active in the total oxidation of CVOCs include supported noble metals, bulk or supported transition metal oxides, transition metal doped micro and mesoporus solids, as well as classical acid catalysts such as Al_2O_3, zeolites or TiO_2/SiO_2 [3,6–36]. Supported precious metal catalysts have been recognized as most active and selective to the desired reaction products [3,6,7]. However, due to high costs and sensitivity to poisoning of the noble-metal based systems, other catalytic materials, especially those containing transition metals, represent an attractive alternative. Of the latter, Cr based catalysts have been reported to be the most active, although aspects associated with possible formation of toxic products, such as chromium oxychloride, have to be considered [7].

Of special importance for the outcome of CVOC oxidation is the nature of the support, which, when properly chosen, may enhance both the reaction efficiency and the catalyst stability. Thus, it has been shown that the use of acidic supports, e.g., γ-alumina or zeolites, facilitates catalytic combustion of chlorinated organics because the surface acid sites act as effective chemisorption centers for halocarbons [7–10]. On a titania-supported catalyst Windawi and Zhang [12] observed a direct correlation between the light-off temperature and the energy required for rupture of the C—Cl bond in the CVOC to be oxidized, which has been taken as an indication of an involvement of a radical mechanism. Several reports point to the favorable support-active phase interactions operating at the surface of chemically robust zirconia or titania-containing carriers [27–33]. However, in contrast to the most frequently used γ-alumina support, it is difficult to prepare TiO_2 or ZrO_2 as high surface area, thermally stable and resistant to sintering materials.

This prompted us in the past to design the CVOCs oxidation catalysts using titania- and/or zirconia-pillared natural montmorillonite clays in the capacity of the active phase carriers [21,34–36]. Clay pillaring is a procedure which consists in propping open the clay layers (typically by 0.5–2 nm) by exchanging the interlayer charge-compensating cations with bulky oligomeric polyoxymetal cationic species. Upon thermal treatment, the oligomers form oxide clusters that link permanently the clay layers, and render the interlayer space open to potential reactants. The expanded, highly porous and thermally stable material, possessing intrinsic acidity, is referred to as pillared interlayered clay, abbreviated PILC. A number of reviews of catalytic applications of PILCs point to the ever increasing use of these materials as catalytic supports [36–45]. Zirconia and/or titania pillars located in the PILC interlayer constitute oxide materials of unique properties, combining high surface to bulk ratio associated with the nanometer size of pillars, with resistance to sintering ensured by the lateral spacing of oxide props and firm bonding to the clay layer. Another advantage of a PILC support is the material acidity, expected to facilitate chemisorption of halocarbons.

There are several reports in the open literature on the application of catalysts based on pillared clays to the destruction of CVOCs [11,14,21,36,46–51]. Most of them describe the use of Al-, Cr- or Fe-pillared montmorillonites as CVOCs oxidation catalysts or catalyst supports [11,14,46–51]. Those stemming from our group show results obtained for Ti-PILC-based systems, and demonstrate that such catalysts are much more efficient than the commercial alumina-supported noble metal reference [21,36]. On the basis of these findings, patented catalytic systems involving Ti- and Zr-PILC materials have been developed in our laboratory [34,35].

Recently, we have shown that mixed [Ti,Zr]-pillared montmorillonite represents a different quality with respect to Ti- and Zr-pillared clays, as far as structural, textural, electronic and acid–base properties are concerned [52]. In view of the significance attributed to the role of support, we decided to investigate the performance of CVOCs oxidation catalysts containing noble metal and/or transition metal-based active phase supported on Ti-, Zr- or mixed [Ti,Zr]-pillared montmorillonites. Palladium and/or chromium have been chosen as active redox components representing noble and non-noble transition metals. Dichloromethane (DCM) and trichloroethylene (TCE), both representing major aliphatic organochlorine pollutants, were selected as model CVOCs. The compounds differ with respect to the ease of destruction [53], as well as the hydrogen/chlorine ratio, affecting the efficiency of HCl formation. In view of the above, the chosen compounds represent sensitive probes of the versatility of Pd and/or Cr-doped pillared cays as catalysts for CVOCs combustion.

2. Experimental

2.1. Materials

Montmorillonite used in this study was the sodium form of the less than 2 μm particle size fraction separated by sedimentation from Milowice bentonite (Poland), washed free of chloride ions by dialysis, referred to as Na-mt. The cation exchange capacity of the clay is 84 meq per 100 g. Zr-pillared clay was obtained following the approach of Yamanaka and Brindley [54], using aqueous solution of $ZrOCl_2{\cdot}8H_2O$ (Fluka, analytical grade) as a pillaring agent, while Ti-pillared material was synthesized according to the method of Sterte [55], refined by Bernier et al. [56], with pillaring solution obtained by partial hydrolysis of $TiCl_4$ (Aldrich, pure, ≥98%). Pillaring agent for preparation of montmorillonite intercalated with zirconium and titanium polycations mixture was obtained by mixing the Ti- and Zr-pillaring solutions in required proportions. Detailed synthetic procedures are described in our previous works [52,57]. The as-received materials after freeze-drying were referred to as Zr-mt, Ti-mt, [Ti,Zr]-mt, and after calcination at 400 °C for 3 h, as Zr-PILC, Ti-PILC, and [Ti,Zr]-PILC, respectively. 1 wt.% of palladium, chromium or simultaneously palladium and chromium (in 1:1 weight ratio) were introduced by incipient wetness impregnation with appropriate quantities of $Cr(NO)_3{\cdot}9H_2O$ (POCH, analytical grade) aqueous solution and/or $PdCl_2$ (POCH, analytical grade) aqueous solution acidified with few drops of concentrated HCl to achieve complete dissolution of Pd salt. The resulting wet cake was freeze dried and calcined at 500 °C for 3 h. The obtained catalysts are referred to as Pd-X-PILC, Cr-X-PILC and (Pd,Cr)-X-PILC, where X: Zr, Ti or [Ti,Zr].

2.2. Methods

X-ray diffraction patterns were recorded with a Philips APD PW 3020 X'Pert diffractometer with CuKα radiation and graphite monochromator. The samples were analyzed in the range of $2\theta = 2–73^\circ$ with a constant step of 0.05°.

Chemical composition of investigated solids was determined with an Orbis Micro-EDXRF analyzer with a Rh anode as X-ray source (operating at 30 kV and 500 mA) and Si(Li) detector, using Orbis Vision software. The system allows for multi-element detection for elements from sodium to uranium.

Scanning electron microscopy (SEM) analysis was carried out with aid of JEOL JSM-7500F microscope coupled with INCA PentaFetx3 EDS system. The secondary electron detector provided SEI images and back scattered electron detector provided BSE (COMPO) micrographs.

Transmission electron microscopic (TEM) studies were performed with FEI Tecnai G^2 transmission electron microscope at 200 kV equipped with EDX and HAADF/STEM detectors.

X-ray photoelectron spectroscopy (XPS) spectra were obtained with a hemispherical analyzer (SES R4000, Gammadata Scienta, pass energy 100 eV). The Al Kα X-ray source (1486.6 eV) was applied to generate core excitation. The system was calibrated according to ISO 15472:2001. The analysis area of the sample (powder pressed into indium foil) was about 3 mm^2. The electron binding energy scale (BE) was calibrated for maximum of C 1s core excitation at 285.0 eV. The spectra were fitted with the Casa XPS 2.3.12 software, using Gaussian/Lorentzian functional (70:30) and Shirley-type background.

ESR spectra were recorded at room temperature and at −196 °C with a conventional X-band SE/X (Technical University Wroclaw) spectrometer.

Temperature programmed reduction (TPR) of calcined samples was performed in a quartz U-type tubular reactor using a TCD as detector. Quantachrome CHEMBET 3000 apparatus was applied. A 15-mg sample was used. The reducing gas was a mixture of 5 vol.% H_2 in Ar (Linde, H_2 5% in Ar), at a total flow rate of 30 ml min^{-1}. The temperature was increased at a rate of 10 °C min^{-1} from room temperature to 650 °C.

Textural parameters were derived on the basis of N_2 adsorption/desorption measurements performed at −196 °C with the use of Quantachrome AUTOSORB 1 instrument in the relative pressure range from $\sim 6.6 \times 10^{-6}$ to 0.9975. Prior to the measurement the samples were outgassed at 200 °C for 3 h. The *t* method was used for specific surface area (S^t) calculations [58]. The total pore volume (V_{tot}) was calculated from the amount of adsorbed N_2 at a relative vapor pressure (p/p_o) close to 1.0. Microporosity was assessed by applying the *t* method, the mesoporosity from the adsorption branch of the isotherms by using the BJH method. The mean diameter of all pores (D_{av}) was calculated with the use of $D_{all} = 4V_{tot}/S^t$ equation.

The overall surface acidity of the samples was studied by temperature programmed desorption of ammonia (NH_3-TPD). The measurements were performed in a flow microreactor system equipped with a QMS detector (Stanford Research, RGA 200). Desorption of ammonia was studied by monitoring the $m/z = 16$ line and $m/z = 17$ line, corrected for the contribution from water mass spectrum. Prior to ammonia sorption, the sample was outgassed in a flow of pure argon at 400 °C for 1 h. Subsequently, the microreactor was cooled down to 100 °C and the sample was saturated in a flow of NH_3 for about 30 min. Then, the sample was purged with argon flow until a constant baseline level was attained. Physically adsorbed ammonia was removed in a flow of argon at 110 °C for 2 h. Desorption was carried out with a linear heating rate (10 °C/min) in a flow of pure argon, in the temperature range 50–600 °C, at a 10 °C/min heating rate.

Determination of the nature of the acid sites was carried out by a FTIR study of pyridine adsorption (POCh Gliwice, analytical grade, dried over 3 A molecular sieve). Absorption spectra were recorder for self-supporting pellets of PCH samples. The pellet was placed in a quartz cell equipped with CaF_2 windows, designed to perform measurements at different temperatures. Prior to pyridine adsorption, the sample was outgassed at 400 °C under vacuum for 1 h. Then the cell was cooled to room temperature and the spectrum of activated sample was obtained. Later the sample was allowed to interact with pyridine at room temperature. Thereafter the cell with a sample was outgassed for 20 min under vacuum at 170 °C. After cooling down, the FTIR spectra of the samples were measured. For each measurement 64 scans were taken with a resolution of 2 cm^{-1} using a Nicolet 710 FTIR spectrometer. To assess quantitatively the amount of adsorbed pyridine species, difference spectra were obtained by subtracting the spectrum of activated sample from spectrum obtained after pyridine adsorption. Concentrations of Brønsted acid sites, Lewis acid sites, and hydrogen-bonded pyridine were calculated (in μmol/g) on the basis of the intensities of the 1545–1547 cm^{-1}, 1454–1448 cm^{-1} and 1445 cm^{-1} bands, respectively [59]. Following absorption coefficients were used: $\epsilon(PyH^+) = 0.078$ cm/μmol, $\epsilon(PyL) = 0.165$ cm/μmol and ϵ(Py—hydrogen-bonded) = 0.165 cm/μmol.

Catalytic activity in DCM and TCE oxidation was measured in a fixed-bed flow quartz reactor of 10 mm inner diameter, loaded with 0.5 g of a catalyst (particle size 0.3–0.5 mm), in the temperature range 200–550 °C. DCM or TCE was fed to the air stream containing 10% water vapor, at a concentration of 2 g/m^3 (STP) (530 and 340 ppm, respectively). The GHSV was 10,000 h^{-1}. The reaction products, except of HCl, Cl_2, CO_2 and CO, were analyzed by an on-line GC (SRI 86 10A) with a DCQF-1 column. CO and CO_2 were analyzed by GC (Chrom-5) with TCD and two columns: HayeSep R for CO_2 and molecular sieve 5 A for CO. HCl was analyzed by bubbling a known volume of the effluent stream through a trap with distilled water followed by conductivity measurement of the HCl solution. Cl_2 was determined by bubbling a known volume of the effluent stream through a trap with KI solution, followed by titration of the liberated iodine with $Na_2S_2O_3$ solution. For the sake of comparison the catalytic tests were also carried out for a commercial $Pt,Pd/Al_2O_3$ catalyst suitable for CVOCs oxidation, manufactured by Süd-Chemie.

3. Results and discussion

3.1. Characterization of catalysts

3.1.1. XRD analysis and N_2 adsorption/desorption isotherms

Detailed characterization of Ti-PILC, Zr-PILC and [Ti,Zr]-PILC pillared clay supports used in this study has been presented in a separate paper [52]. In this work we focus on the effects induced by deposition of the catalytically active transition metal oxides. Impregnation with 1 wt.% of Cr and/or Pd does not affect the XRD pattern of supports in any meaningful way, as illustrated in Fig. 1a on the example of [Ti,Zr]-PILC-based series. The data on the effect of impregnation with Pd and/or Cr on textural characteristics of supports are gathered in Table 1. The table also shows the values of d_{001} basal spacing and the content of pillar-forming oxides in PILC carriers. It should be noted that the specific surface areas calculated from *t*-plot (S^t) are considered more appropriate when comparing isotherms of different types [57]. PILC supports are essentially microporous, as ca. 80% of their specific surface area is generated by pores <20 Å, whose average diameters grow in the order Zr-PILC < [Ti,Zr]-PILC < Ti-PILC. Noteworthy, the average micropore dimensions reported in Table 1 are larger than the heights of interlayer determined by the size of introduced polycations. Subtraction of the smectite layer thickness of 9.6 Å from the d_{001} of pillared samples yields gallery heights of 10.7, 6.8 and 13.9 Å, for [Ti,Zr]-PILC, Zr-PILC and Ti-PILC, respectively, which is less than the corresponding average micropore diameters of 15.1, 14.4 and 19.5 Å. The effect is attributed to the contribution from micropores formed at the interparticle contacts between smallest montmorillonite platelets [52]. Isotherms of Cr and/or Pd doped materials retain the character typical of pure supports (Fig. 1b). Thus, isotherms of catalysts related to [Ti,Zr]-PILC and Zr-PILC are of mixed type I/type II, while those of catalysts belonging to the Ti-PILC family are of type II, due to the fact that micropores generated in Ti-PILC are distinctly larger and enable multilayer adsorption. All samples show very narrow H4 hysteresis loops, determined by the presence of platy particles and slit-shaped pores. Doping with Cr and/or Pd of Zr-PILC and [Ti,Zr]-PILC causes a minor downward shift of the isotherms with respect to pure supports (Fig. 1b) and a slight decrease of the specific surface area and textural parameters associated with microporosity (Table 1), which suggests that a portion of dopants is located within the micropore system or at the micropore mouth.

Table 1
Textural parameters, content of intercalated pillar material, and d_{001} values of Ti-PILC, Zr-PILC and [Ti,Zr]-PILC before and after doping with Pd and/or Cr.

Sample	S^t [m²/g]	$S_{mic.}{}^t$ [m²/g]	$V_{mic.}{}^t$ [cm³/g]	V_{tot} [cm³/g]	D_{mic} [Å]	D_{mes} [Å]	D_{av} [Å]	Isotherm loop	d_{001} [Å]	ZrO_2 [wt.%]	TiO_2 [wt.%]
Ti-PILC	379	298	0.145	0.392	19.5	144.3	41.4	II/H4	23.5	–	31.2
Pd-Ti-PILC	392	314	0.156	0.399	19.9	132.3	40.7	II/H4	23.5	n.d.	n.d.
Cr-Ti-PILC	379	300	0.151	0.411	20.1	144.3	43.4	II/H4	23.5	n.d.	n.d.
(Pd,Cr)-Ti-PILC	378	296	0.148	0.396	20.0	130.5	41.9	II/H4	23.5	n.d.	n.d.
Zr-PILC	267	217	0.078	0.254	14.4	78.3	38.0	I/II/H4	16.4	12.9	–
Pd-Zr-PILC	248	194	0.071	0.216	13.1	72.6	34.8	I/II/H4	16.4	n.d.	n.d.
Cr-Zr-PILC	239	188	0.067	0.217	13.8	70.2	36.3	I/II/H4	16.4	n.d.	n.d.
(Pd,Cr)-Zr-PILC	246	197	0.063	0.236	12.8	65.5	38.4	I/II/H4	16.4	n.d.	n.d.
[Ti,Zr]-PILC	379	322	0.122	0.361	15.1	79.4	38.1	I/II/H4	20.3	11.9	8.2
Pd-[Ti,Zr]-PILC	342	287	0.108	0.361	15.0	74.0	42.2	I/II/H4	20.3	n.d.	n.d.
Cr-[Ti,Zr]-PILC	349	291	0.105	0.407	14.4	70.4	46.6	I/II/H4	20.3	n.d.	n.d.
(Pd,Cr)-[Ti,Zr]-PILC	352	296	0.113	0.374	15.2	78.6	42.5	I/II/H4	20.3	n.d.	n.d.

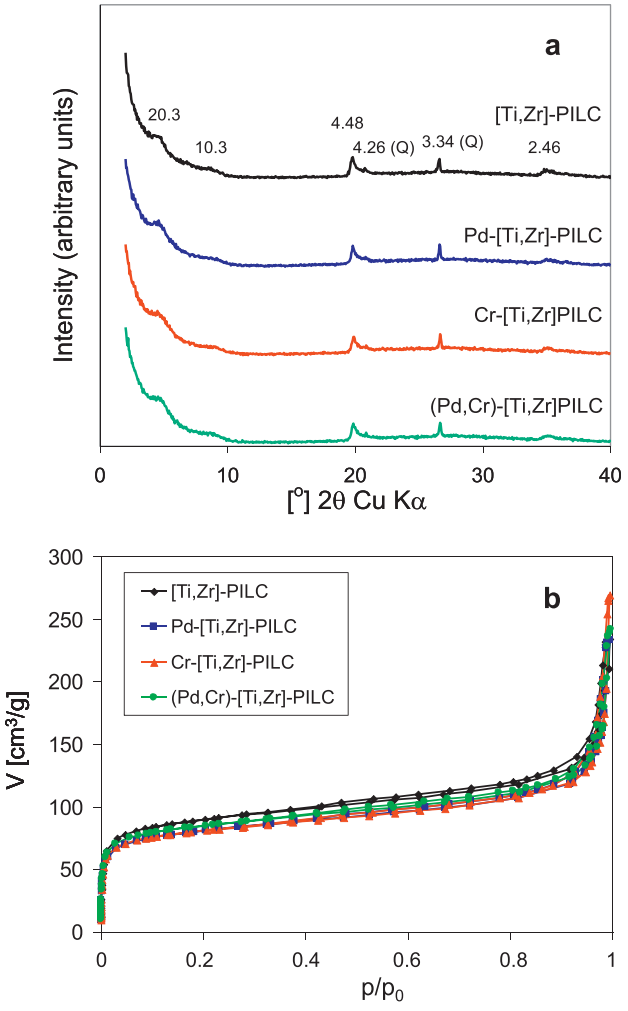

Fig. 1. (a) XRD patterns and (b) N_2 adsorption/desorption isotherms of [Ti,Zr]-PILC support, and Pd-[Ti,Zr]-PILC, Cr-[Ti,Zr]-PILC, and (Pd,Cr)-[Ti,Zr]-PILC catalysts.

However, it should be noted that the observed differences remain within the margin of error of the isotherm measurement. In the case of Cr and/or Pd impregnated Ti-PILC support, with larger average diameter of micropores, the values of textural parameters, in particular those characterizing microporosity, show no important differences with respect to the undoped matrix. Here, the data show no diminishing trend, but are scattered within ±10% of the initial figures characteristic of Ti-PILC. Thus, it may be concluded that the adopted procedure of pillared clay doping with the transition metal active phase does nor affect the structural and textural properties of the support in any meaningful way.

High specific area and porosity displayed by PILC-supported catalysts are particularly advantageous from the point of view of their application in the complete combustion reactions, in which the transformation to final products requires eventual dissociation of substrates to individual atoms. This multistep process goes through a number of intermediates and requires a whole sequence of transformations at the surface of a catalyst [60]. High porosity favors multiple contacts of reagents with surface active centers, thus enabling the reaction to reach completion.

3.1.2. SEM and TEM analyses

SEM analysis of the catalysts has been carried out in SEI and COMPO modes. The former is based on low energy secondary electrons emerging from near to surface area, and provides a probe of material's morphology. The COMPO mode is based on backscattered electrons, sensitive to the material density (or atomic number), therefore, it enhances the image of areas containing heavy elements, which appear brighter than the background. This is illustrated in Fig. 2, which shows microphotographs obtained for the Pd-Ti-PILC, Pd-Zr-PILC and Pd-[Ti,Zr]-PILC catalysts. SEI image, presented in Fig. 2a, shows that pilllared clay catalysts are composed of randomly oriented flaky particles characteristic of montmorillonite support. In Fig. 2b–f, recorded in COMPO mode, the heavy Pd-containing particles appear as brighter dots and can be distinguished from the less dense support material. The images show that impregnation leads to the formation of PdO_x nanoparticles spread over the surface of support, the size of individual grains detectable by SEM/COMPO images being predominantly in the range of 3–10 nm. Occasionally, particles of dimensions up to 20 nm appear, but no larger aggregates can be found in the analyzed material, which points to good dispersion of palladium. However, it should be noted that at the surface of [Ti,Zr]-PILC the population of bigger, 10–20 nm PdO_x particles appears to be more numerous (Fig. 2d) than in the case of Ti-PILC (Fig. 2b) or Zr-PILC (Fig. 2c). However, the larger grains coexist with the copious amount of very fine PdO_x particles visible at higher magnification (Fig. 2e). TEM analysis confirms SEM findings as to the dominating sizes of PdO_x particles, as illustrated in Fig. 3a for Pd-Zr-PILC. In addition, TEM study reveals that the catalysts contain also PdO_x species smaller than 3 nm (Fig. 3b). Fig. 3c and e shows, respectively, representative HRTEM images of smaller and bigger palladium-containing nanoparticles with visible lattice fringes. Analysis of the corresponding SAED patterns indicates that palladium exists in the catalysts as nanocrystals of PdO. The appearance of PdO nanoparticles implies that, upon impregnation, a hydrolytic transformation of Pd^{2+} occurs and polymeric rather than monomeric palladium species become attached to the support [61,62]. Contrary to palladium catalysts, the CrO_x

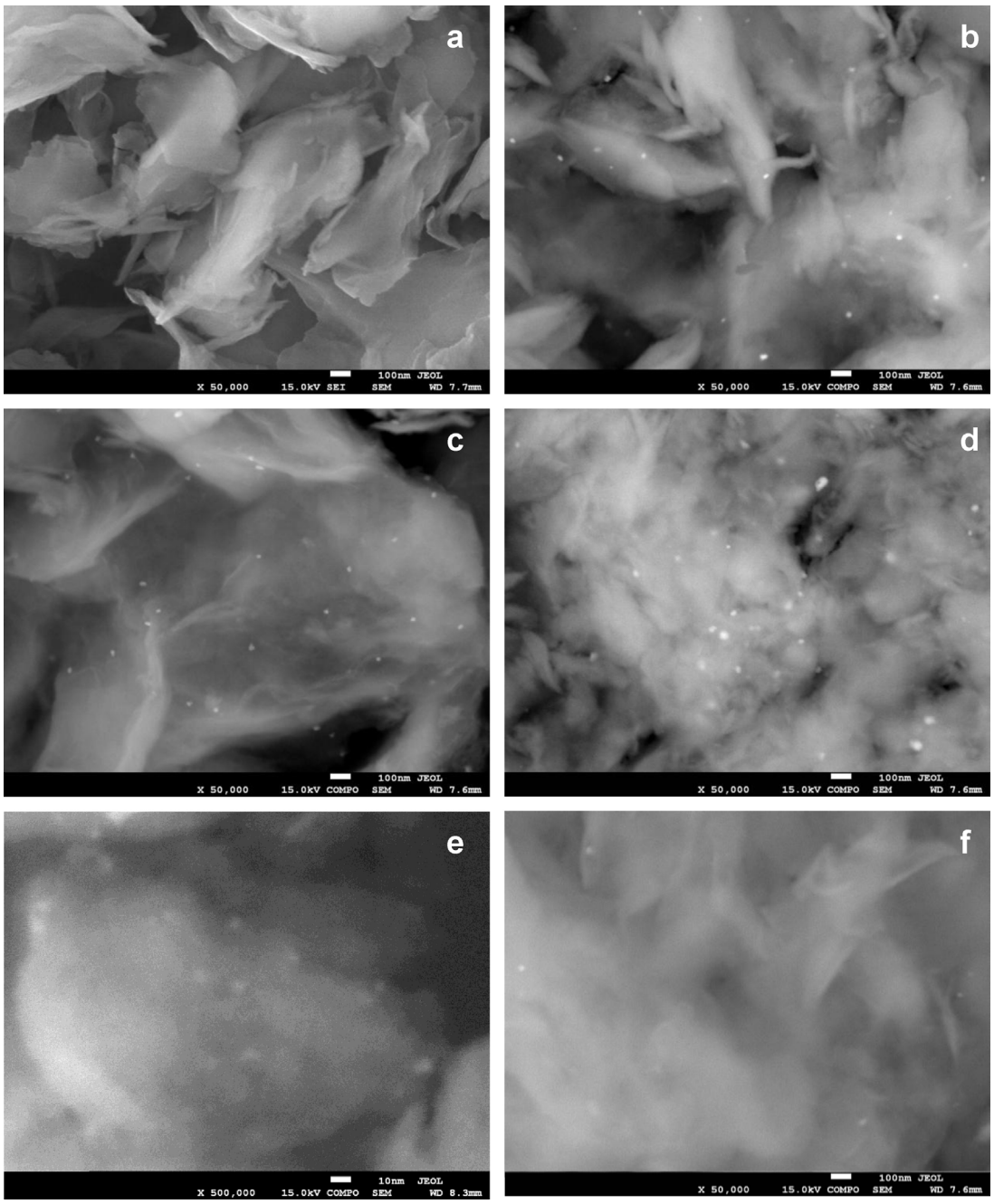

Fig. 2. SEM images of (a) Pd-Ti-PILC catalyst, SEI mode, ×50,000, (b) Pd-Ti-PILC catalyst, COMPO mode, ×50,000, (c) Pd-Zr-PILC catalyst, COMPO mode, ×50,000, (d) Pd-[Ti,Zr]-PILC catalyst, COMPO mode, ×50,000, (e), Pd-[Ti,Zr]-PILC catalyst, COMPO mode, ×500,000, and (f) (Pd,Cr)-Zr-PILC catalyst, COMPO mode, ×50,000.

species present in the Cr-doped pillared clay samples are not distinguishable from the support background in SEM/COMPO images. This may be taken as an indication of higher dispersion of supported chromium phase. In fact, it is a general view that calcined supported chromium oxide systems with low Cr loading contain predominantly isolated mono- and/or dichromate-like species [63]. The nature of CrO_x species will be further discussed in Sections 3.1.3 and 3.1.4. In SEM/COMPO images of catalysts with mixed (Pd,Cr) active phase, obtained by impregnation with a solution containing both transition metal dopants, the bigger PdO particles, of ≥10 nm size, appear much less numerous, even if one takes into account that the absolute content of palladium is half of that present in materials containing Pd dopant only (Fig. 2f). This suggests that upon co-impregnation the PdO particles become better dispersed. The effect may be related to the hydrolytic equilibria of Pd^{2+} and attributed to the lower concentration of palladium in the solution employed for co-impregnation. As observed by Milić and Bugarčić [62] the extent of Pd^{2+} ion hydrolysis drops with decreasing concentration of palladium, hence the formation of smaller PdO particles upon impregnation with more diluted solution.

3.1.3. *Raman spectroscopy*

Raman spectroscopy is particularly suitable to study supported metal oxide catalysts, due to its ability to probe molecular vibrations at low wavenumbers, where metal oxides exhibit characteristic absorptions [64]. The Raman spectra of Cr-doped catalysts show a peak at 865–869 cm^{-1}, as illustrated by the spectrum of Cr-[Ti,Zr]-PILC in Fig. 4. Other, low intensity peaks visible in the

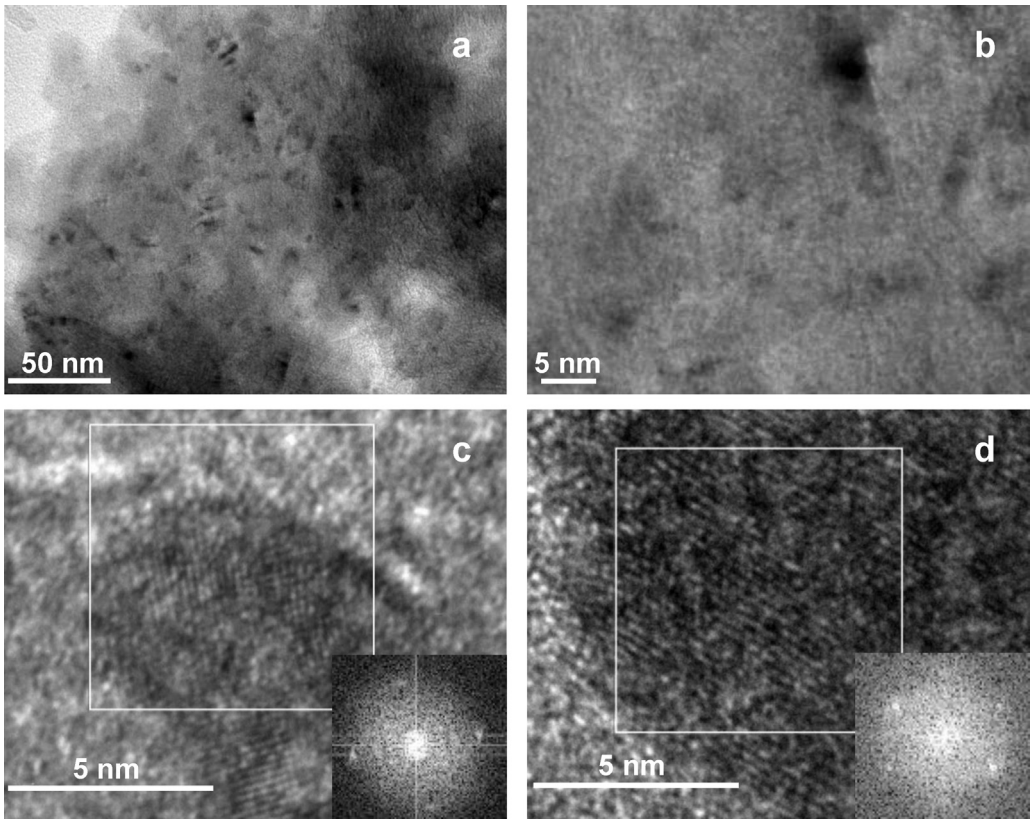

Fig. 3. (a) and (b) TEM images of Pd-Zr-PILC, (c) HRTEM image of Pd-Zr-PILC showing a <5 nm PdO nanocrystal with the corresponding SAED pattern, and (d) HRTEM image of Pd-Zr-PILC showing a >10 nm PdO nanocrystal with the corresponding SAED pattern.

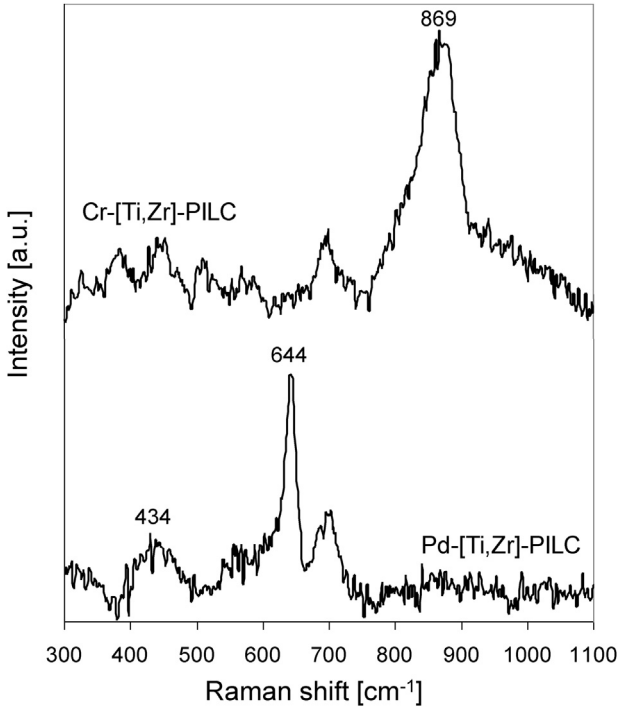

Fig. 4. Raman spectra of (a) Cr-[Ti,Zr]-PILC, and (b) Pd-Zr-PILC.

spectrum are due to the pillared clay support. The appearance of a band around 865 cm^{-1} is considered a fingerprint of hydrated monochromates [63], and shows that such species dominate at the surface of pillared clay catalysts impregnated with 1 wt.% of chromium. The asymmetry of this band is most likely caused by different locations of chromate species within the pillared clay structure, while the increased background intensity in the range 900–1100 cm^{-1} may point to the contribution from vibrational modes of polymeric chromate species. In the case of palladium supported on Zr-PILC and [Ti,Zr]-PILC, a narrow band at 642 and 644 cm^{-1}, respectively, appears, as illustrated in the example presented in Fig. 4. This band may be attributed to the Raman active B_{1g} phonon mode of PdO [65]. In the case of Pd-Ti-PILC the B_{1g} band is completely obscured by the much stronger band at 651 cm^{-1} originating from anatase-like titania pillars (not shown) [52]. It has been shown that in the nanocrystals of PdO the B_{1g} mode becomes red-shifted with respect to bulk PdO where it is observed at 651 cm^{-1} [66]. The effect is due to confinement of phonons within nanocrystal grain boundaries, and its magnitude increases with the decreasing size of PdO nanocrystals. Thus, the red shift of the PdO B_{1g} bands with respect to the value characteristic of bulk PdO, observed in this work, confirms the nanocrystalline character of PdO species supported on pillared clay carriers.

3.1.4. X-ray photoelectron spectroscopy

High resolution XP spectra in the electron binding energy regions corresponding to Pd 3d and Cr 2p core excitations provide additional information about the structure and electronic properties of transition metal dopants in the pillared clay catalysts. Upon deconvolution of the spectra three types of palladium species have been found at the surface of pillared clay supports. $3d_{5/2}$ bands with the lowest observed binding energy, 336.8–336.9 eV, are denoted A and attributed to Pd^{2+} ions in the PdO-like environment [67,68]. They appear only on Ti-PILC support, where they constitute the majority palladium species. In addition, two types of surface Pd^{4+} centers, referred to as B and C, exist in the catalysts. Species C is

Table 2
XPS parameters of palladium species in Pd-containing pillared clay catalysts.

Sample	Spectrum component	BE Pd $3d_{5/2}$ [eV]	%Area	Species
Pd-Ti-PILC	A	336.8	65.0	Pd^{2+}
	B	339.1	35.0	Pd^{4+}
Pd-Zr-PILC	C	337.4	33.6	Pd^{4+}
	B	339.3	66.4	Pd^{4+}
Pd-[Ti,Zr]-PILC	C	337.4	62.1	Pd^{4+}
	B	339.5	37.9	Pd^{4+}
(Cr,Pd)-Ti-PILC	A	336.9	56.3	Pd^{2+}
	B	339.1	43.7	Pd^{4+}
(Cr,Pd)-Zr-PILC	C	338.0	34.5	Pd^{4+}
	B	339.3	65.5	Pd^{4+}
(Cr,Pd)-[Ti,Zr]-PILC	C	337.9	62.5	Pd^{4+}
	B	339.2	37.5	Pd^{4+}

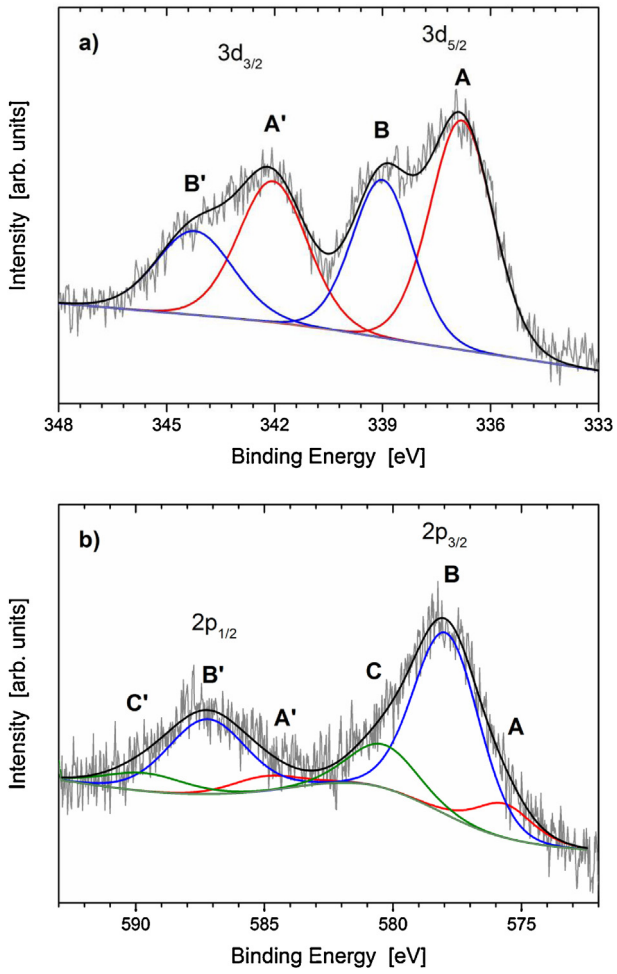

Fig. 5. Examples of deconvolution and fitting of XPS spectra: (a) Pd 3d in Pd-Ti-PILC, (b) Cr 2p in Cr-Zr-PILC.

characterized by the binding energies 337.4–338.0 eV, which fall into the range of values reported for Pd $3d_{5/2}$ in PdO_2 [67,68]. Species B, with BE in the range 339.1–339.5 eV, can be assigned to Pd^{4+} in the $Pd(OH)_4$-like surrounding [69]. B and C forms of Pd^{4+} are the only surface palladium species found on Zr-PILC and [Ti,Zr]-PILC supports. The XPS parameters and speciation of palladium centers are gathered in Table 2. The Pd 3d core level spectrum of Pd-Ti-PILC sample, together with the deconvolution details, is shown, as an example, in Fig. 5a. Thus, the XPS analysis shows that although,

Table 3
XPS parameters of chromium species in Cr-containing pillared clay catalysts.

Sample	Spectrum component	BE Cr $2p_{3/2}$ [eV]	%Area	Species
Cr-Ti-PILC	A	575.2	6.5	Cr^{3+}
	B	577.9	77.7	Cr^{5+}/Cr^{6+}_{pillar}
	C	580.6	15.8	Cr^{6+}_{clay}
Cr-Zr-PILC	A	575.1	12.4	Cr^{3+}
	B	577.6	65.0	Cr^{5+}/Cr^{6+}_{pillar}
	C	579.7	22.6	Cr^{6+}_{clay}
Cr-[Ti,Zr]-PILC	A	575.6	12.0	Cr^{3+}
	B	577.9	70.6	Cr^{5+}/Cr^{6+}_{pillar}
	C	580.4	17.4	Cr^{6+}_{clay}
(Cr,Pd)-Ti-PILC	A	576.2	12.6	Cr^{3+}
	B	577.9	62.5	Cr^{5+}/Cr^{6+}_{pillar}
	C	580.3	24.8	Cr^{6+}_{clay}
(Cr,Pd)-Zr-PILC	A	576.7	21.2	Cr^{3+}
	B	577.6	61.8	Cr^{5+}/Cr^{6+}_{pillar}
	C	581.1	59.3	Cr^{6+}_{clay}
(Cr,Pd)-[Ti,Zr]-PILC	A	576.3	16.5	Cr^{3+}
	B	578.2	59.8	Cr^{5+}/Cr^{6+}_{pillar}
	C	581.1	23.7	Cr^{6+}_{clay}

according to HRTEM and Raman spectroscopy, palladium exists as PdO particles, only in Pd-Ti-PILC Pd^{2+} represents the majority surface species. In Pd-Zr-PILC and Pd-[Ti,Zr]-PILC, the surface of PdO particles is oxidized and contains exclusively Pd^{4+} species.

Analysis of Cr 2p core level spectra shows that in all samples satisfactory fitting between the experimental and the simulated data, can be obtained by deconvolution of the spectrum into three components (Fig. 5b), whose XPS parameters and assignment are given in Table 3. It is now generally accepted that in calcined supported chromium oxide systems with low Cr loading chromium is present predominantly as dispersed chromate-like Cr^{6+} species, with little or no contribution from Cr^{3+} [63]. Accordingly, the component A, assigned to Cr^{3+} ions on the basis of binding energy (575.1–575.6 eV, in samples containing only Cr, and 576.2–576.7 eV in samples containing Cr and Pd) [67,68], represents minority species. The two other components, of higher binding energies, confirm that the majority Cr species represent highly oxidized chromium ions. While the component C, characterized by $2p_{3/2}$ binding energy 579.7–581.1 eV, can be assigned to Cr^{6+} centers of the chromate type [67,68], the dominant spectrum component, referred to as B, with binding energies in the range 577.6–578.2 eV is less straightforward to interpret. It may point to the presence of Cr^{5+} [70,71] frequently identified in calcined supported chromium oxide [63] and/or to the occurrence of Cr^{6+} with a decreased effective charge, e.g., due to the more covalent nature of Cr—O-surface bonding. The former possibility is confirmed by ESR analysis, which shows that in all calcined Cr-containing catalysts a strong, sharp, symmetric spectrum with $g_{av} = 1.97$ appears (Fig. 6a), characteristic of isolated, mononuclear Cr^{5+} [72,73]. The second option is also likely, because in PILC materials the anchored chromate species, depending on their location (pillars or clay layers), may be linked to the surface via oxygen bridges with metal centers of different electronegativities (values after Allred [74] in parentheses): Cr(1.66)–O–Ti(1.54), Cr(1.66)–O–Zr(1.33), Cr(1.66)–O–Al(1.61), or Cr(1.66)–O–Si(1.90). Based on XPS measurements of oxides, a phenomenological view has been formulated by Barr [75] and confirmed by ab initio DFT–LDA calculations of Guittet et al. [76], that in the mixed oxide bonding system the cation of more ionic oxide becomes even more ionic (i.e., its effective charge increases), while that of more covalent oxide experiences an increase of covalency (i.e., its effective charge becomes lower). In view of this, the Cr centers bonded via oxygen bridge to Ti and/or Zr sites should acquire a more covalent character and become less positive, while the

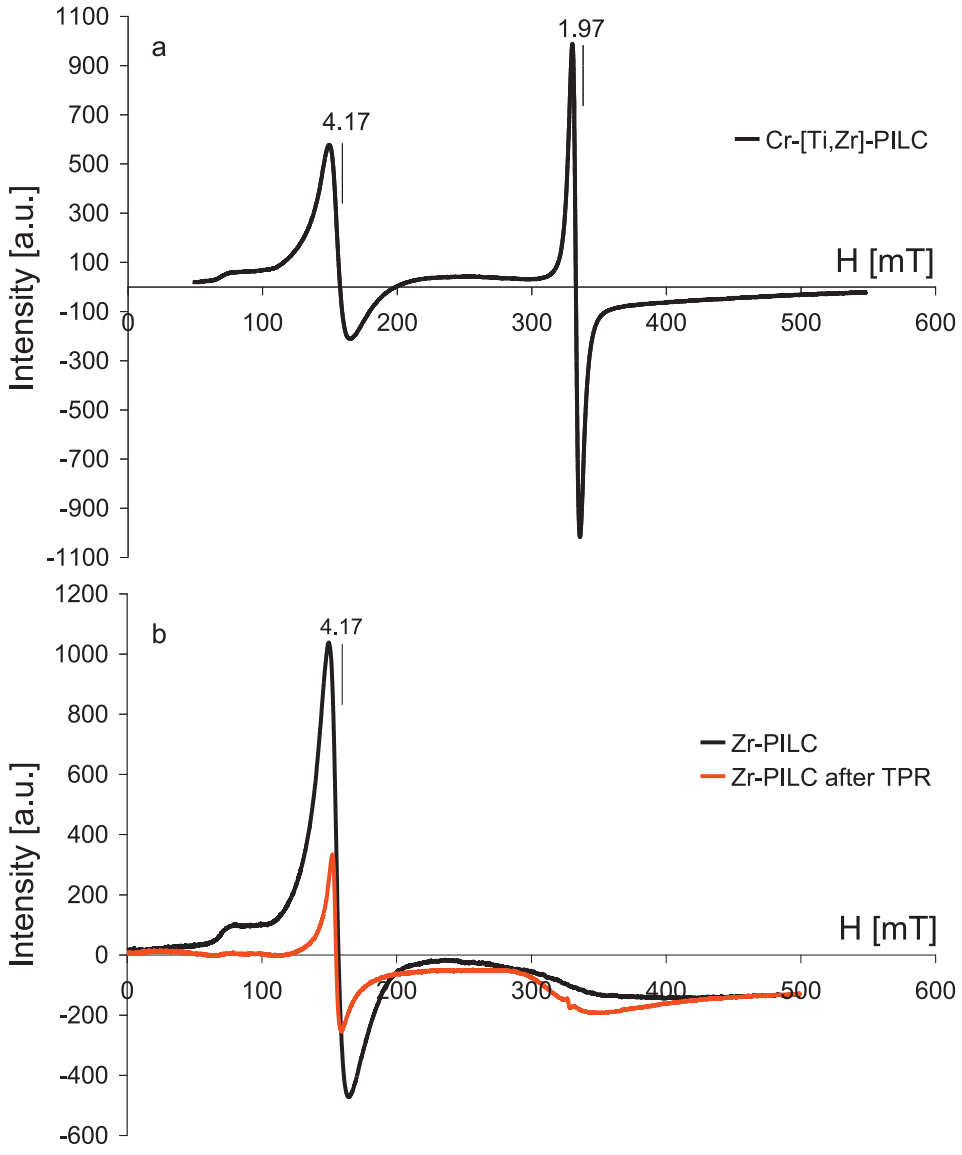

Fig. 6. ESR spectra of (a) Cr-[Ti,Zr]-PILC catalyst, recorded at −196 °C, and (b) Zr-PILC support before and after TPR run, recorded at −196 °C.

opposite effect should occur for Cr sites linked to Si. In consequence, the binding energy of Cr attached to pillars should be lower than that of chromium bonded to silicon sites in clay layers. The above reasoning prompted us to interpret the component B as due to the joint input from Cr^{5+} ions, and Cr^{6+} centers anchored to Ti, Zr or [Ti,Zr] pillars. Consequently, we attribute the component C to Cr^{6+} species linked to the silica sheet of clay layer.

Thus, in general, the XPS analysis shows that in calcined catalysts the surface palladium or chromium species exist preferably in their highest, or next to highest, oxidation states. Only on Ti-PILC, the dominant form of surface palladium is Pd^{2+}. In view of the XPS, HRTEM and Raman analyses, the stoichiometry of Pd-containing nanoparticles may be presented as $PdO_{x(x\geq 1)}$.

3.1.5. Temperature programmed reduction with hydrogen

Reducibility of the clay-derived catalysts, an important factor influencing their activity in oxidation reactions, has been investigated by means of the temperature programmed reduction with hydrogen, in the temperature range 25–650 °C. Results are presented in Fig. 7, together with TPR runs recorded for the relevant PILC supports. The TPR profiles of all PILC carriers are similar. The main effect is the high temperature maximum, occurring around 600 °C, associated with the reduction of structural iron, present in the parent montmorillonite as Fe^{3+} ions substituting Al^{3+} in the octahedral sheet [77]. This interpretation is confirmed by the EPR analysis of the samples before and after TPR run. Structural Fe^{3+}, located in the environment of highly distorted octahedral symmetry, produces a low-field signal near $g = 4$ [78]. In the present study, the reducing treatment experienced by pillared clay supports results in a distinct decrease of structural Fe^{3+} signal intensity, which proves participation of these centers in the hydrogen uptake (Fig. 6b).

In the case of PILC-supported palladium catalysts (red lines in Fig. 7), irrespective of the pillar nature, the first TPR effect observed upon increase of the temperature is a negative H_2-consumption. This phenomenon, frequently encountered in palladium catalysts, is due to the fact that already at ambient temperature, upon equilibration in the hydrogen flow, reduction of PdO_x species to Pd metal, followed by absorption of hydrogen to yield palladium hydride, may occur [79]. As the temperature goes up, PdH_x decomposes, and the accompanying release of hydrogen is reflected in the TPR curve as a negative hydrogen uptake. This effect is responsible for the minima appearing in the range 70–80 °C on TPR profiles of Pd-Ti-PILC, Pd-Zr-PILC and Pd-[Ti,Zr]-PILC. It has been pointed out that

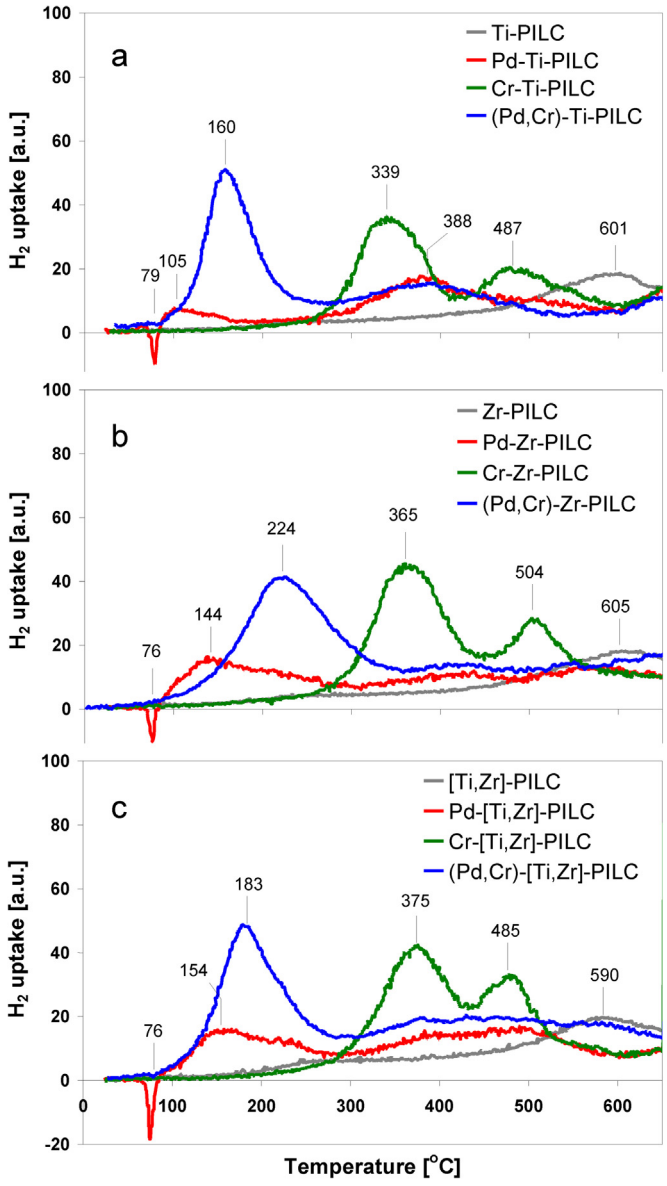

Fig. 7. TPR profiles of (a) Ti-PILC and related supported Pd and/or Cr catalysts, (b) Zr-PILC and related supported Pd and/or Cr catalysts, and (c) [Ti,Zr]-PILC and related supported Pd and/or Cr catalysts. (For interpretation of the references to color in the text, the reader is referred to the web version of this article.)

the magnitude of the hydrogen release peak depends on the dimensions of supported palladium particles, because the tendency to form the hydride phase decreases with increasing dispersion of Pd [80]. Analysis of the TPR profiles in Fig. 7 shows that the negative peak is most pronounced in the case of Pd-[Ti,Zr]-PILC, suggesting that palladium present in this catalyst is somewhat less dispersed than in Pd-Ti-PILC and Pd-Zr-PILC. This conclusion is consistent with the results of SEM analysis, which shows that bigger PdO_x nanoparticles can be found more easily in Pd-[Ti,Zr]-PILC than in the two other members of the series, and with Raman analysis of this sample showing a smaller red shift of the PdO B_{1g} mode. The next effect is a positive H_2 uptake, attributed to the reduction of PdO_x species which have not been reduced at room temperature. In supported Pd catalysts such an enhanced resistance to reduction is usually attributed to a strong interaction of PdO_x particles with the support [81,82]. Noteworthy, for Pd-Ti-PILC the maximum of this effect occurs at much lower temperature (105 °C) than in the case of both Pd-Zr-PILC and Pd-[Ti,Zr]-PILC (144 and 154 °C, respectively), pointing to the better reducibility of PdO_x deposited on Ti-PILC support. This is consistent with the results of XPS analysis of calcined catalysts, which indicates that Ti-PILC is the only support favoring formation of Pd^{2+} rather than Pd^{4+}. The lower initial oxidation state of palladium in Pd-Ti-PILC is also reflected in the lower hydrogen uptake associated with reduction of PdO_x particles, observed for this catalyst. Once the palladium metal is formed, the dissociative chemisorption of H_2 molecules into more reactive H atoms, and their subsequent migration over the surface of the catalysts, known as hydrogen spillover, enhances the reduction processes in the studied systems [83]. Thus, in all Pd-containing PILC samples the high temperature maximum attributed to the reduction of clay structural Fe^{3+} ions disappears. Instead, a hydrogen uptake smeared over the temperature range 300–550 °C occurs, which confirms that reduction of Fe^{3+} with spilt over hydrogen species is a more facile process. Moreover, the magnitude of hydrogen consumption in this temperature range is higher in Pd-Ti-PILC and Pd-[Ti,Zr]-PILC than in Pd-Zr-PILC, which suggests, that some reduction of Ti^{4+} present in titania, or mixed titania–zirconia pillars takes place. However, it should be born in mind that, although the TPR results allow comparison of the strength of lattice oxygen bonding in the Pd-containg catalysts, the effects due to the hydrogen spillover will be absent under conditions of catalytic combustion.

All calcined Cr-impregnated pillared clay supports, show similar TPR profiles, composed of two distinct maxima of hydrogen consumption. Bearing in mind the highly oxidized state of these samples revealed by XPS, the first, more intense hydrogen uptake, is assigned to the reduction of Cr^{6+} (and Cr^{5+}) to Cr^{3+} [14,70,84–89]. The temperatures of these maxima show a distinct influence of the support on the reducibility of deposited chromium. Similarly as in the case of palladium dopant, chromium-containing catalysts are most reducible when supported on Ti-PILC carrier (T_{max} = 339 °C) and most difficult to reduce on [Ti,Zr]-PILC (T_{max} = 375 °C). Reducibility on Zr-PILC (T_{max} = 365 °C) assumes an intermediate value, but it is much closer to that of [Ti,Zr]-PILC than to Ti-PILC. The next TPR maximum, of lower intensity, may be attributed either to the reduction of another, less reducible type of Cr^{6+} species [86], or, to further reduction of Cr^{3+} formed in the first step, to Cr^{2+} [84,85,88,89]. If all supported chromium were in the highest oxidation state, the overall hydrogen consumption should correspond to 3H atoms per chromium center in the case of reduction to Cr^{3+}, while 4H atoms per chromium site would be required to form Cr^{2+} as the final state of a TPR run. In the present work the H/Cr ratio, calculated from the observed hydrogen uptake, after subtracting contribution from the overlapping Fe^{3+} reduction, is 3.2, 3.5 and 3.9 for Cr-Ti-PILC, Cr-Zr-PILC and Cr-[Ti,Zr]-PILC, respectively. Bearing in mind that, according to XPS and EPR, not all chromium is in the oxidation state +6, these figures suggest that the reduction of Cr^{3+} to Cr^{2+} is a more likely explanation of the origin of the second TPR maximum. In fact, XPS analysis of Cr-containing samples after the TPR run confirms the presence of Cr^{2+} in the reduced material. The lack of the high temperature maximum attributed to the reduction of structural Fe^{3+} ions in pillared clay support suggests that, similarly as in Pd-doped catalysts, this effect is shifted to lower temperatures and overlaps with the hydrogen uptake by chromium species. Such result indicates that deposited CrO_x species are capable of activating hydrogen and facilitating reduction of iron in clay layers. Activation of hydrogen by supported chromium oxide, leading to the downward shift of TPR maxima associated with the reduction of the support, was also reported by Hoang and Lieske [87].

TPR profiles of samples containing both Pd and Cr are similar in character for all studied supports, but represent a new quality with respect to catalysts containing only one transition metal dopant. It should be noted, that hydrogen consumption is dominated by

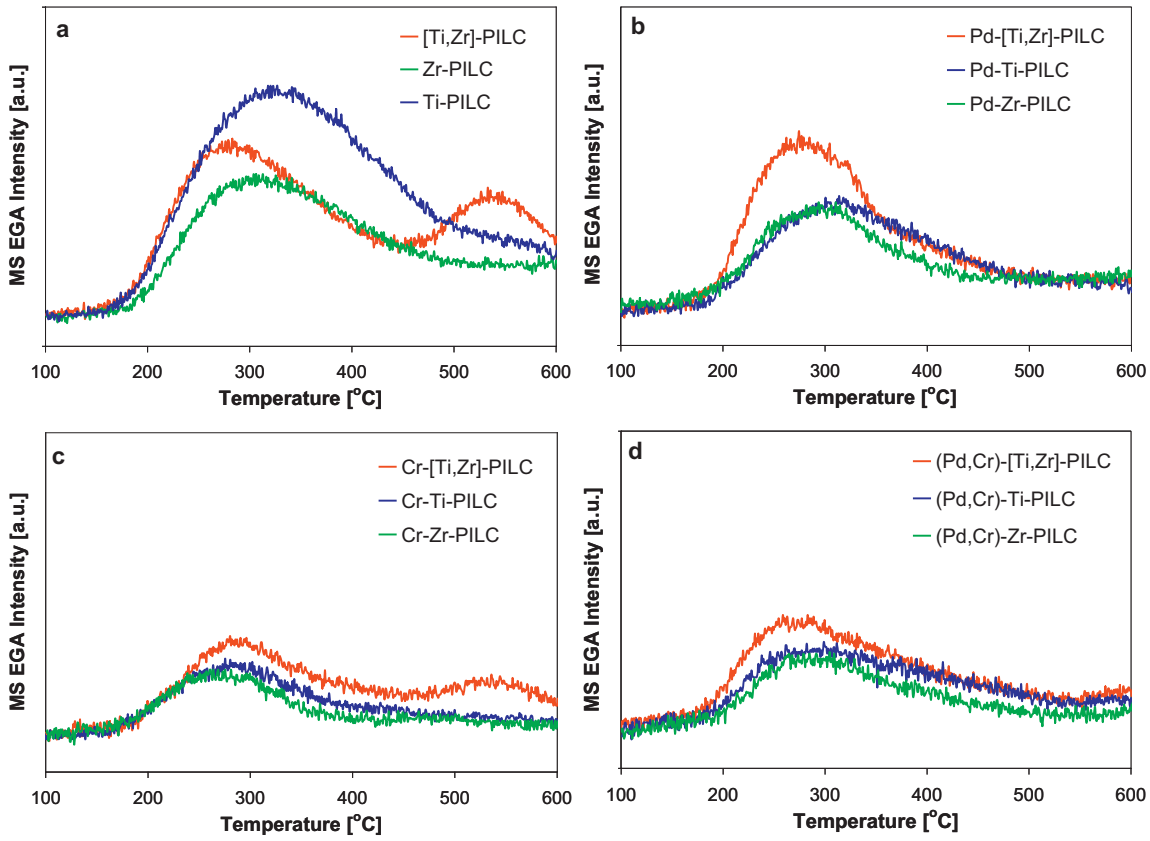

Fig. 8. TPD of ammonia from the surface of (a) [Ti,Zr]-PILC, Ti-PILC, Zr-PILC (b) Pd-[Ti,Zr]-PILC, Pd-Ti-PILC, Pd-Zr-PILC, (c) Cr-[Ti,Zr]-PILC, Cr-Ti-PILC, Cr-Zr-PILC, and (d) (Pd,Cr)-[Ti,Zr]-PILC, (Pd,Cr)-Ti-PILC, (Pd,Cr)-Zr-PILC.

the effects associated with chromium, because the Cr/Pd weight ratio equal 1, corresponds to Cr:Pd atomic ratio equal 2. A strong, single, low temperature maximum is observed below 300 °C, followed by a broad, flat effect, extended over the temperature range 300–550 °C. The latter, is attributed to the reduction of clay structural Fe^{3+} with hydrogen species spilt over from palladium and/or with hydrogen activated by CrO_x species. The low temperature maximum encompasses all reduction phenomena associated with the Pd and Cr dopants. It is obvious that the coexistence of palladium and chromium species leads to a spectacular modification of the redox charactertistics of single components. In particular, the reduction steps $Cr^{6+}(Cr^{5+}) \rightarrow Cr^{3+} \rightarrow Cr^{2+}$ coalesce and shift strongly to lower temperatures, so that they overlap with the effects of PdO_x reduction. The latter occurs without the formation of palladium hydride, as inferred from the lack of the negative hydrogen uptake. Since, as mentioned earlier, formation of hydride is favored by the presence of larger Pd particles, this result supports the observation made already by SEM analysis, that a better dispersion of PdO_x occurs when the supports are impregnated jointly with Pd and Cr. The enhancement of chromium species reduction in the presence of palladium is attributed to the action of reactive hydrogen atoms generated by dissociation of hydrogen molecules at the metallic palladium sites followed by their spillover to the catalyst surface [83]. Similar phenomena have been known since long in systems containing palladium and other transition metal components [90]. For this reason, the H_2 TPR experiment carried out on Pd,Cr-containing samples bears no direct relation to the redox behavior of these catalysts under conditions of catalytic combustion, where the hydrogen spillover effect is absent. The positions of the hydrogen uptake maxima show that, similarly as in the case of single Cr dopant, chromium species supported on Ti-PILC are most reducible.

3.1.6. Acidity measurements

In view of the significance of acid–base properties of the catalysts for the interaction with halocarbons, the assessment of materials acidity has been carried out by means of ammonia TPD and adsorption of pyridine monitored by FTIR. Our earlier study [52] of Ti-, Zr-, and [Ti,Zr]-pillared clays used for the preparation of the Pd and/or Cr supported catalysts, showed that the materials acidity is predominantly of the Lewis type, in agreement with other literature reports on PILC [37,91–94]. [Ti,Zr]-PILC was singled out as support with a significant population of Lewis acid sites much stronger than those present in either Ti-PILC or Zr-PILC materials.

Fig. 8 shows the NH_3 TPD–MS profiles of pillared clay supports before (a) and after impregnation with Pd and/or Cr (b–d). It is clear that deposition of transition metal dopants brings about a decrease of the overall acidity as compared to pure supports, in the order PILC > Pd-doped > (Pd,Cr)-doped > Cr-doped samples. For each type of the active phase, the catalysts prepared with the [Ti,Zr]-PILC support show highest total acidity.

The nature of acid sites present in the catalysts was identified by adsorption/desorption of pyridine monitored by FTIR spectroscopy. Depending on the type of interaction, three forms of adsorbed pyridine may exist at the surface of an acidic solid: (a) pyridinium ion, which results from the transfer of an acidic proton from the surface Brønsted site to the pyridine molecule, (b) pyridine coordinatively bonded through its nitrogen lone pair to the surface Lewis acid site, and (c) hydrogen bonded pyridine which is formed due to the interaction of its nitrogen lone pair with hydrogen of the relatively acidic surface hydroxyls. In the present study, the IR bands at 1545–1547 cm^{-1}, 1454–1448 cm^{-1} and 1445 cm^{-1} have been taken as indicative of the presence of pyridinium ion, Lewis center coordinated pyridine and H-bonded pyridine, respectively [59]. The data on the content of particular forms of adsorbed pyridine

Table 4
FTIR determined concentration of various pyridine species bonded to the catalysts surface after outgassing at 170 °C.

Sample	Brønsted acid centers	Lewis acid centers	H-bonded pyridine
Ti-PILC	110	275	50
Pd-Ti-PILC	21	105	–
Cr-Ti-PILC	16	58	–
(Pd,Cr)-Ti-PILC	15	69	–
Zr-PILC	126	145	28
Pd-Zr-PILC	19	98	–
Cr-Zr-PILC	8	42	–
(Pd,Cr)-Zr-PILC	11	55	–
[Ti,Zr]-PILC	101	211	19
Pd-[Ti,Zr]-PILC	20	138	–
Cr-[Ti,Zr]-PILC	14	76	–
(Pd,Cr)- [Ti,Zr]-PILC	15	91	–

remaining at the surface of investigated materials after desorption at 170 °C are presented in Table 4. The results of pyridine adsorption confirm that after impregnation of PILC supports with Pd and/or Cr a decrease of acidity is observed. FTIR shows that the concentrations of all types of pyridine binding sites are affected, albeit to a different degree. Thus, upon impregnation, the weakly acidic hydroxyls which bind pyridine via hydrogen bonding are completely eliminated, and the content of Brønsted acid sites is reduced to ≤20% of the value found in pure supports. The concentration of Lewis acid sites is also lowered but to a lesser extent. The observed effects of the active phase deposition are likely to be associated, at least in part, with the fact that surface hydroxyl groups participate in binding of the transition metal to the support [63]. It should be noted that, in the conditions of impregnation, the hydrolysis of Lewis acid sites occurs, leading to the formation of surface hydroxyls [95], which increases the population of sites capable of transition metal ion anchoring. Similarly as in the case of ammonia TPD, also pyridine adsorption data demonstrate that, irrespective of the nature of the active phase, the highest overall acidity is obtained for the catalysts prepared with the [Ti,Zr]-PILC support.

3.2. Catalytic oxidation of DCM and TCE

Activities of the Pd-, Cr- and (Pd,Cr)-containing PILC catalysts in the combustion of DCM and TCE are presented in Figs. 9 and 10, respectively, in the form of conversion vs. temperature profiles. For comparison, each diagram shows also the results obtained for one of the undoped PILC supports. In addition, Fig. 9a and Fig. 10a include the activity data for the reference commercial supported noble metal catalyst. From Figs. 9 and 10, it is evident, that although pure supports show some activity in the oxidation of chlorinated pollutants, it is the addition of transition metal dopants that renders the systems extremely active in destruction of CVOCs. No products other than HCl, Cl_2, CO_2 and CO were detected. Both for DCM and TCE the carbon balance was consistently over 90% in the whole range of studied temperatures, while chlorine balance was in the range 75–90% below 300 °C, and over 90% above this temperature. In order to facilitate the ranking of the catalysts, the T_{50} and T_{90} values, i.e., the temperatures of 50% and 90% conversion, are gathered in Table 5, together with the information on the corresponding selectivities to the undesired reaction products, Cl_2 and CO. Table 5 also contains information on the performance of the reference commercial catalyst. Noteworthy, the diagrams presented in both figures, as well as the data in Table 5, show that all PILC-supported catalysts are much more active in combustion of model CVOCs than the commercial reference.

Analysis of the DCM combustion results shows that, for a given type of support, the catalysts containing only Cr are the most active ones (Fig. 9, Table 5), while the Pd- and (Pd,Cr)-doped PILCs perform in a comparable manner. Hence, in DCM combustion the

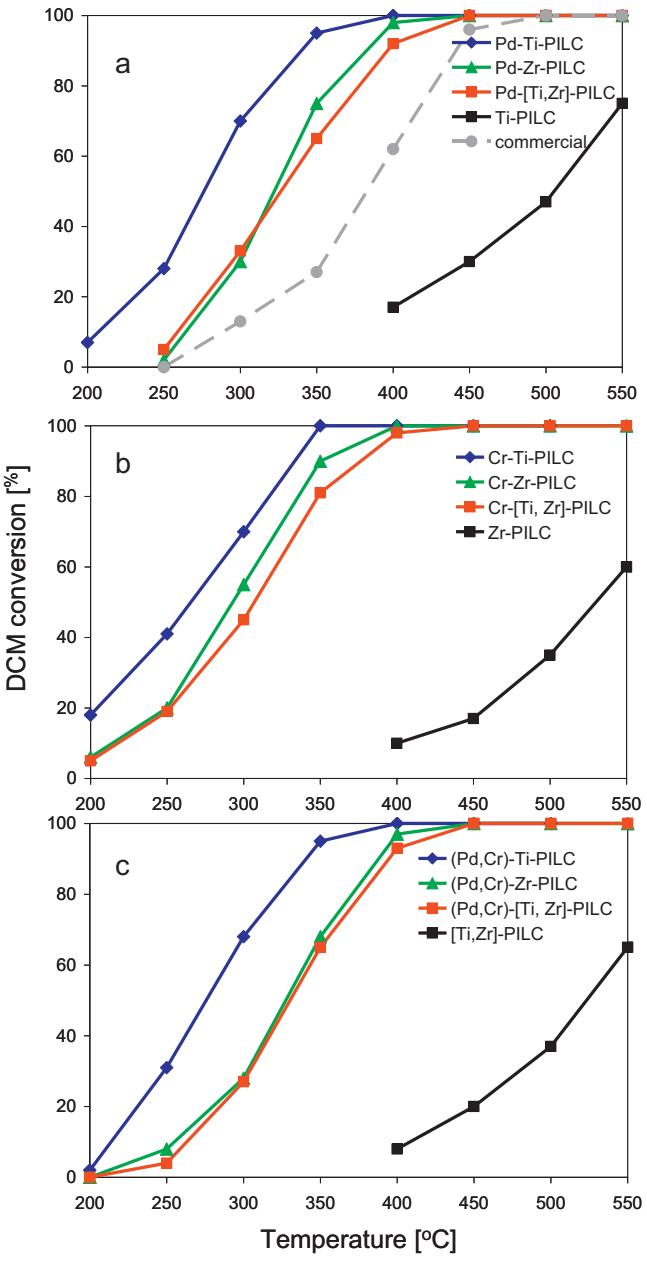

Fig. 9. Activity of Pd- and/or Cr-doped pillared clays in destruction of DCM.

ranking of catalytically active components is Cr > (Pd,Cr) ≅ Pd. High activity of Cr-containing catalysts in CVOCs combustion has long been well recognized and attributed to the availability of multiple valences coupled with large ionization potentials of chromium cations in higher oxidation states [14,96–105]. While comparing activity of palladium and chromium based catalysts, it appears that, in the present work, the factor of key importance is the high dispersion of chromium active phase, combined with the fact that for equal weight content of the dopant, there is twice as many Cr centers in the catalyst as Pd ones. As demonstrated by Raman spectroscopy, CrO_x species exist at the pillared clay support surface predominantly in the form of monochromates. On the other hand, Raman and SEM/TEM analyses show that palladium is present in the form of PdO nanocrystals, in which only surface palladium species may be directly involved in the catalytic reaction. It is also advantageous that chromium supported on PILCs assumes, as shown by XPS and ESR, high oxidation state $Cr^{5+/6+}$, rather than

Table 5
Temperatures of 50% and 90% conversion and selectivities to chlorine and CO at 50% and 90% conversion for pillared clay supported Pd and/or Cr catalysts.

Sample	DCM						TCE					
	T_{50} [°C]	S_{50}^{Cl2} [%]	S_{50}^{CO} [%]	T_{90} [°C]	S_{90}^{Cl2} [%]	S_{90}^{CO} [%]	T_{50} [°C]	S_{50}^{Cl2} [%]	S_{50}^{CO} [%]	T_{90} [°C]	S_{90}^{Cl2} [%]	S_{90}^{CO} [%]
Pd-Ti-PILC	275	0	0	339	0	0	309	0	0	371	1	0
Pd-Zr-PILC	322	0	0	383	1	0	306	0	0	359	0	0
Pd-[Ti,Zr]-PILC	325	0	0	395	0	0	269	0	0	339	0	0
Cr-Ti-PILC	265	6	24	332	32	28	261	2	10	295	15	48
Cr-Zr-PILC	297	0	11	350	10	20	255	0	21	293	7	26
Cr-[Ti,Zr]-PILC	306	0	1	372	4	8	242	0	4	288	8	34
(Pd,Cr)-Ti-PILC	275	0	0	337	6	0	300	0	0	338	13	0
(Pd,Cr)-Zr-PILC	326	3	0	380	10	0	289	0	4	338	0	0
							290[a]	0	3	342[a]	0	0
(Pd,Cr)-[Ti,Zr]-PILC	329	0	0	393	9	0	265	0	0	328	4	0
Commercial Pt,Pd/Al_2O_3	378	2	0	438	24	0	370	1	0	426	19	0

[a] After longevity test at 400 °C.

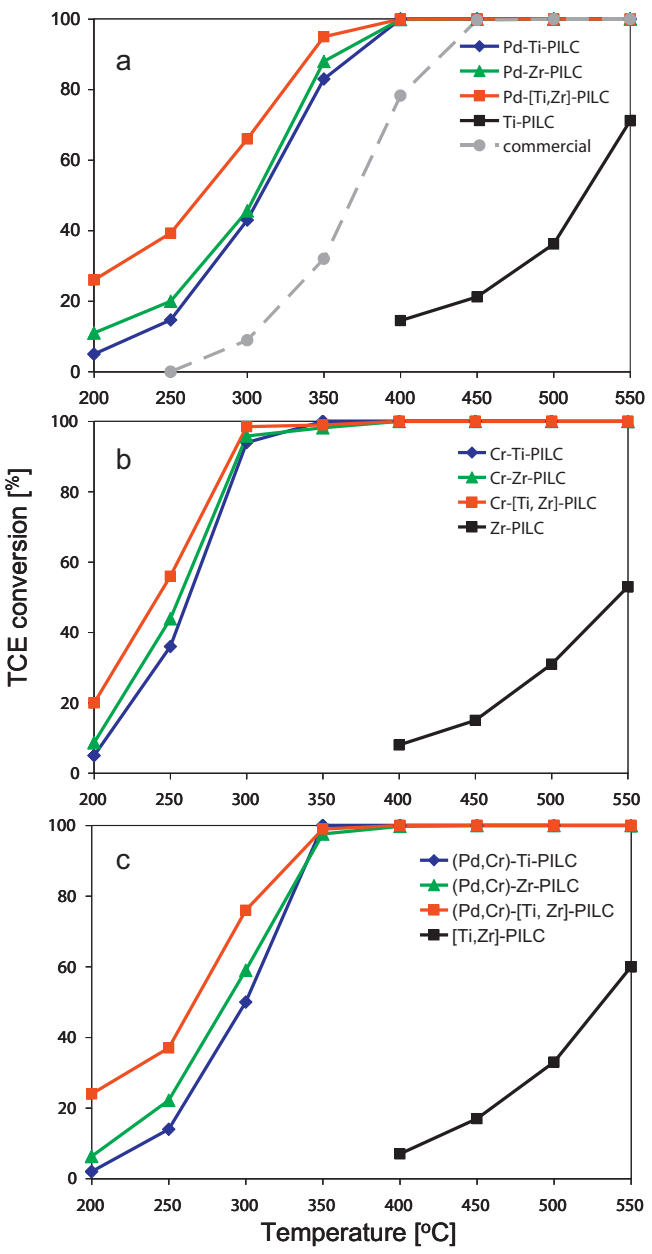

Fig. 10. Activity of Pd- and/or Cr-doped pillared clays in destruction of TCE.

Cr^{3+}. It has been repeatedly demonstrated that the presence of chromium in the high oxidation state is essential for the efficient mediation of the redox cycle during catalytic combustion of CVOCs [14,48,97,99,103,105].

Comparison of conversion vs. temperature profiles in Fig. 9, and the T_{50} and T_{90} data in Table 5, shows yet another consistent pattern: for the catalysts with the same type of the active phase, the highest activity in DCM combustion is always obtained for Ti-PILC support. The use of two other supports gives comparable activities, the Zr-PILC carrier yielding slightly more active catalysts. Thus, the order of PILC supports in terms of their beneficial influence on the course of DCM combustion is Ti-PILC > Zr-PILC ≥ [Ti,Zr]-PILC. While looking for a rationale explaining this trend, it should be recalled that literature data point to catalyst acidity and/or reducibility as chief catalytic functions influencing the efficiency of hydrocarbon destruction. Acid sites are considered effective chemisorption centers for the chlorinated hydrocarbon molecule, at which dehydrochlorination occurs, while redox centers are involved in the oxygen insertion step required for the formation of deep oxidation products. In the case of DCM, it has been shown that the first step is the interaction of a chlorine atom with surface acidic OH group, followed by release of HCl and formation of chloromethoxy intermediate [106–108]. Sinquin et al. [107] pointed out that the oxygen required for further transformation of the chloromethoxy group comes from the catalyst lattice. This type of oxidation is known as Mars van Krevelen mechanism [109]. In this mechanism the true oxidizing agents are reducible cations, while the oxygen species inserted into the oxidation product are the nucleophilic lattice oxide ions. The oxygen vacancies thus formed are replenished by subsequent reaction with gaseous oxygen, which restores also the high oxidation state of cations.

While analyzing the influence of the nature of the PILC support on the catalyst activity in the DCM combustion, no obvious relation to the results of acidity measurements is observed. However, the activity trend reflects the results of TPR experiments, which show that the ease of oxygen extraction from palladium and chromium active phases depends on the support nature and decreases in the order Ti-PILC > Zr-PILC > [Ti,Zr]-PILC. Therefore, it appears, that in the case of DCM combustion over PILC-supported Pd and/or Cr catalysts, the strength of lattice oxygen binding, rather than the surface acidity, plays the key role in determining the catalyst activity.

Monitoring of the product distribution shows that the only Cl-containing products of DCM combustion are HCl and Cl_2, while carbon is oxidized to CO_2, and, in few cases, to CO. Table 5 shows the selectivities to the undesired products, chlorine and CO, at 50% and 90% conversions. The stoichiometry of DCM enables formation

of hydrogen chloride from constitutional hydrogen and chlorine atoms, according to the equation:

$$CH_2Cl_2 + O_2 \rightarrow CO_2 + 2HCl$$

Chlorine may appear as a result of HCl oxidation, known as the Deacon reaction:

$$2HCl + 1/2O_2 \leftrightarrow H_2O + Cl_2$$

Indeed, on many catalysts, especially those containing chromium, evolution of molecular chlorine is observed upon increase of the reaction temperature, leading to enhanced Cl_2 selectivity at 90% conversion (Table 5). Clearly, palladium catalysts stand out as those capable of an efficient conversion of chlorine contained in DCM to the desired hydrogen chloride, and at nearly complete combustion show none (on Ti-PILC and [Ti,Zr]-PILC) or almost none (on Zr-PILC) formation of Cl_2. In contrast, Cr-containing samples produce substantial amount of Cl_2. Cr-Ti-PILC, which is most active in DCM combustion, is also most active in catalyzing oxidation of HCl. In the case of catalysts with mixed (Pd,Cr) active phase, the S_{90}^{Cl2} values are intermediate between those observed for the Pd-only and Cr-only catalysts. The attractive feature of the most active catalyst in this group, (Pd,Cr)-Ti-PILC, is the high activity (comparable to that of Pd-only counterpart), combined with the relatively low S_{90}^{Cl2} value (6%). Noteworthy, the reference commercial catalyst produces more chlorine at 90% conversion than any of the PILC-supported samples, except of Cr-Ti-PILC.

As far as CO_2 and CO formation is concerned, all catalysts containing palladium, either as the sole dopant or in mixture with Cr, show 100% selectivity to CO_2 in the whole range of studied temperatures. Also on the reference catalyst no emission of CO is observed. In the case of supported Cr catalysts, formation of CO, next to CO_2, is observed. As reported by Greene et al. [98], CO is an intermediate in the formation of carbon dioxide, and on Cr-based catalysts the process of its transformation to CO_2 becomes effective only at higher temperatures. Indeed, at temperature $\geq$450 °C carbon monoxide disappears completely from the reaction products over Cr-based catalysts.

The light-off curves obtained for combustion of TCE are shown in Fig. 10. The conversion vs. temperature profiles and the T_{50} and T_{90} parameters (Table 5) show that, also in the case of TCE combustion, the PILC-supported catalysts perform much better than the commercial reference. Again, for a given type of support, the active phase containing only Cr gives clearly the best performance. The (Pd,Cr)-doped PILCs perform better than those containing only Pd, but the T_{50} and T_{90} values in Table 5 show that the difference between them is always smaller than between any of these catalysts and the corresponding sample with purely Cr active phase. Interestingly, despite the fact that TCE is considered particularly recalcitrant CVOC, and, usually, requires higher temperatures for destruction than DCM [53], in the present work, for the majority of the catalysts, the T_{50} and T_{90} values obtained for TCE combustion are lower than those found in oxidation of DCM.

When analyzing the influence of the nature of the support on the course of TCE combustion a pattern, different from that observed in the case of DCM destruction, emerges. Comparison of conversion vs. temperature profiles in Fig. 10, and the T_{50} and T_{90} data in Table 5, shows that for the catalysts with the same type of the active phase, the highest activity in TCE combustion is always obtained for [Ti,Zr]-PILC support, the other two carriers yielding catalysts of lower and mutually comparable activities. This order bears no relation to catalysts reducibility, hence, it appears, that the role of redox properties is overshadowed by the importance of other catalyst properties. Analyzing this effect, one should recall that the chemical characteristics of chloroalkanes and chloroalkenes are quite different [110]. In the case of DCM, a chloroalkane, the feature that determines the molecule reactivity is the presence of a polarized carbon–chlorine bond, whose rupture initiates the oxidative transformation. In the case of chloroalkenes, such as TCE, next to C—Cl bond, the double C=C bond forms another potential center of reactivity. Therefore, for chloroalkenes, interaction with the catalyst surface may occur by formation of π-bonded species. In such a mode of adsorption the chloroalkene molecule acts as a Lewis base coordinating to the surface Lewis acid site [111]. Indeed, in the present work, the enhanced activity of catalysts supported on [Ti,Zr]-PILC correlates with the results of acidity measurements, which show that, irrespective of the nature of the active phase, the highest total acidity, of predominantly Lewis character, is observed for the [Ti,Zr]-PILC support. Thus, we associate the superior activity in TCE combustion of catalysts supported on [Ti,Zr]-PILC with their enhanced ability to adsorb TCE whose double bond acts as a Lewis base.

The molecule of TCE does not contain sufficient number of hydrogen atoms to convert all constitutional chlorine to the desired HCl product. To reach this goal other hydrogen-containing reactants, usually water, have to be co-fed, to enable the occurrence of the process according to the equation:

$$C_2HCl_3 + 3/2\,O_2 + H_2O \rightarrow 2CO_2 + 3HCl$$

As indicated in Section 2, air used for oxidation experiments in the present study contained 10% water vapor. Analysis of TCE oxidation products shows that HCl and Cl_2 are detected as the only Cl-containing products, while carbon is converted to CO_2, and, in few cases, to CO. Table 5 shows the selectivities to the undesired products, chlorine and CO, at 50% and 90% conversions. Similarly as in the case of DCM combustion, catalysts with purely palladium active phase show outstanding selectivity to HCl, and at 90% conversion emit no (Zr-PILC and [Ti,Zr]-PILC) or almost no (Ti-PILC) gaseous chlorine. Again, on Cr-containing samples evolution of chlorine is quite significant, but, in general, S_{50}^{Cl2} and S_{90}^{Cl2} values are lower than in the case of DCM combustion. For the catalysts with mixed (Pd,Cr) active phase, the selectivities to chlorine are lower than for Cr-only catalysts. Noteworthy, at 90% TCE conversion, the (Pd,Cr)-Zr-PILC catalyst shows 100% selectivity to hydrogen chloride, similarly as its Pd-only counterpart, being simultaneously much more active than the latter. All PILC-supported catalysts are more selective to HCl than the commercial reference.

Combustion of carbon part of TCE on catalysts containing palladium as a sole component or in combination with chromium is extremely efficient and at 90% conversion results in 100% selectivity to CO_2, similarly as in the case of the reference commercial catalyst. For supported Cr catalysts, beside CO_2, substantial amounts of carbon monoxide are observed in the reaction products at T_{50} and T_{90}. Upon increase of the temperature above 450 °C carbon monoxide disappears from the reaction products.

The catalysts used for combustion of chlorinated hydrocarbons are known to suffer from deactivation, resulting from exposure to high temperature and contact with aggressive reaction products [112]. Therefore, an experiment has been carried out to test the stability of a PILC-supported catalyst in the reaction of TCE oxidation. The (Pd,Cr)-Zr-PILC sample, showing intermediate activity and good selectivity to the desired reaction products (Table 5), was subjected to 52 h reaction runs at 290 °C, i.e., around temperature of 50% conversion, and at 400 °C, i.e., the temperature ensuring complete combustion (Fig. 11a). Within this period the TCE conversion at 290 °C remained at the same level, while at 400 °C decreased only slightly, from 100% to 97%. Moreover, the catalyst after the longevity trial at 400 °C, subjected to the subsequent test of TCE conversion in the function of temperature, shows performance very similar to that of the fresh sample, as illustrated by the

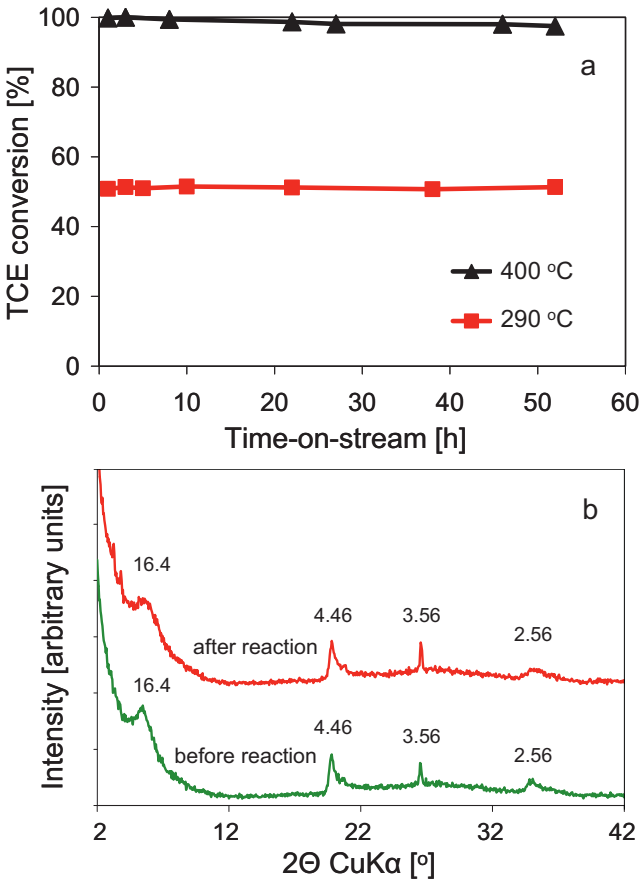

Fig. 11. (a) Test of the (Pd,Cr)-Zr-PILC catalyst stability in the conditions of TCE combustion at 290 and 400 °C, and (b) XRD patterns of the (Pd,Cr)-Zr-PILC catalyst before and after longevity test at 400 °C.

corresponding T_{50} and T_{90} values in Table 5. XRF analysis of the spent catalyst shows that the contents of chromium and palladium remain unaffected by the prolonged exposure to the reaction conditions at 400 °C. Also, no presence of surface chlorine is detected in the survey XPS spectrum of the spent catalyst. These data point to the remarkable resistance of the catalyst to deactivation. The XRD analysis of the catalyst after the 400 °C longevity test showed that its structure bore no evidence of destruction, in particular there was no sign of the pillar collapse, as indicated by the unchanged profile of the d_{001} reflection (Fig. 11b). Also, the specific surface area of the catalyst after the time-on-stream experiment retained high value of 230 m^2/g. These results confirm that zirconia pillars are not only chemically robust, but also, when fixed between the clay layers, resistant to sintering.

4. Conclusions

Palladium and/or chromium catalysts supported on Ti-, Zr- and [Ti,Zr]-pillared montmorillonites represent remarkably active, selective and durable catalytic systems for abatement of chlorinated volatile organics. Detailed physico-chemical characterization of the catalysts shows that deposition of the Pd and/or Cr active phase does not change the essential structural and textural characteristics of the supports and the catalysts constitute high surface area, porous solids. Pd and Cr dopants differ in the degree of dispersion. Palladium is spread over the surface of supports in the form of fine PdO_x nanoparticles, predominantly of $\leq$10 nm size, while chromium is present chiefly as monomeric CrO_x species. Co-impregnation of Pd and Cr improves dispersion of Pd nanoparticles. Surface palladium and chromium species exist preferably in their highest (Pd^{4+}, Cr^{6+}), or next to highest (Cr^{5+}), oxidation states. Only on Ti-PILC the dominant form of surface palladium is Pd^{2+}. Both the palladium- and the chromium-containing catalysts are most reducible when supported on Ti-PILC carrier and most difficult to reduce on [Ti,Zr]-PILC. On the other hand, catalysts supported on [Ti,Zr]-PILC show highest total acidity, of predominantly Lewis character. The characterization data allow relating the excellent catalytic performance of the materials to the combination of highly porous structure of PILC supports, which favors multiple contacts of reactants with active centers on the catalyst surface, good dispersion of the active phase, and appropriate blend of redox and acid–base functions of the catalysts. In both studied catalytic reactions, for a given type of support, the catalysts with Cr-only active phase show best performance in terms of activity. Beside the intrinsic properties of chromium, such as availability of multiple valences and large ionization potentials of cations in higher oxidation states, the factor of key importance in the present work is higher dispersion of Cr active phase as compared to that of Pd, coupled with the absolute chromium content, which, on the atomic basis, is twice that of palladium. The influence of the nature of PILC support on the catalyst activity varies, depending on the type of chlorinated hydrocarbon. In DCM combustion, the superior properties of Ti-PILC support are attributed to the much better reducibility of active phases deposited on this carrier. This points to the determining role of lattice oxygen insertion step in the chain of transformations leading to DCM destruction over PILC supported catalysts. In the oxidation of TCE, best activity is obtained for catalysts supported on [Ti,Zr]-PILC. The effect is correlated with the highest Lewis acidity of these samples, and indicates that TCE interaction with PILC-supported catalysts is governed by the Lewis base character of the double bond.

In terms of selectivity to the desired oxidation products, the Pd-only catalysts are clearly the best. At T_{90} all offer 100% selectivity to HCl and CO_2 for both studied reactions. The most active Cr-only catalysts are least selective, and emit substantial amounts of chlorine and carbon monoxide. Mixed (Pd,Cr)-containing samples represent an attractive, cheaper alternative to purely Pd systems, as at T_{90} their selectivity to CO_2 is 100%, while selectivity to HCl ranges from 87 to 100%, depending on the oxidized chlorocarbon and the nature of PILC support.

Longevity test in the reaction of TCE oxidation, carried out for (Pd,Cr)-Zr-PILC, demonstrated that PILC-supported catalyst is very stable in the reaction environment, both in terms of the catalytic performance and the chemical and structural identity.

Acknowledgments

This work was supported in part by the NCN grant OPUS 2013/09/B/ST5/00983 and AGH University of Science and Technology project 11.11.140.319. R. Janik and W. Rojek are gratefully acknowledged for assistance in carrying out catalytic experiments.

References

[1] L.A. Wallace, Environ. Health Perspect. 95 (1991) 7–13.
[2] H. Sidebottom, J. Franklin, Pure Appl. Chem. 68 (1996) 1757–1769.
[3] J. Spivey, Ind. Eng. Chem. Res. 26 (1987) 2165–2180.
[4] J. Josephson, Environ. Sci. Technol. 18 (1984) 222A–223A.
[5] M.P. Manning, Hazard. Waste 1 (1984) 41–65.
[6] S. Ojala, S. Pitkäaho, T. Laitinen, N. Niskala Koivikko, R. Brahmi, J. Gaálová, L. Matejova, A. Kucherov, S. Päivärinta, C. Hirschmann, T. Nevanperä, M. Riihimäki, M. Pirilä, R.L. Keiski, Top. Catal. 54 (2011) 1224–1256.
[7] A. Aranzabal, B. Pereda-Ayo, M.P. González-Marcos, J.A. González-Marcos, R. López-Fonseca, J.R. González-Velasco, Chem. Pap. 68 (2014) 1169–1186.
[8] S.L. Hung, L.D. Pfefferle, Environ. Sci. Technol. 23 (1989) 1085–1091.
[9] S. Imamura, H. Tarumoto, S. Ishida, Ind. Eng. Chem. Res. 28 (1989) 1449–1452.
[10] S. Chatterjee, H.L. Greene, J. Catal. 130 (1991) 76–85.

[11] L. Storaro, R. Ganzerla, M. Lenarda, R. Zanoni, J. Mol. Catal. A: Chem. 97 (1995) 139–143.
[12] H. Windawi, Z.C. Zhang, Catal. Today 30 (1996) 99–105.
[13] J.A. Rossin, M.M. Farris, Ind. Eng. Chem. Res. 32 (1993) 1024–1029.
[14] L. Storaro, R. Ganzerla, M. Lenarda, R. Zanoni, A. Jiménez López, P. Olivera-Pastor, E. Rodríguez Castellón, J. Mol. Catal. A: Chem. 115 (1997) 329–338.
[15] J.R. González-Velasco, A. Aranzabal, J.I. Gutiérrez-Ortiz, R. López-Fonseca, M.A. Gutiérrez-Ortiz, Appl. Catal. B: Environ. 19 (1998) 189–197.
[16] D. Kiessling, R. Schneider, P. Kraak, M. Haftendorn, G. Wendt, Appl. Catal. B: Environ. 19 (1998) 143–151.
[17] R.W. Van den Brink, P. Mulder, R. Louw, G. Sinquin, C. Petit, J.-P. Hindermann, J. Catal. 180 (1998) 153–160.
[18] A.M. Padilla, J. Corella, J.M. Toledo, Appl. Catal. B: Environ. 22 (1999) 107–121.
[19] J. Janas, R. Janik, T. Machej, E.M. Serwicka, E. Bielańska, E. Bastardo-Gonzalez, W. Jones, Catal. Today 59 (2000) 241–248.
[20] A. Musialik-Piotrowska, K. Syczewska, Catal. Today 73 (2002) 333–342.
[21] K. Bahranowski, A. Gaweł, R. Janik, J. Komorek, T. Machej, A. Michalik, E.M. Serwicka, W. Włodarczyk, Pol. J. Chem. 77 (2003) 675–682.
[22] R. López-Fonseca, S. Cibrián, J.I. Gutiérrez-Ortiz, M.A. Gutiérrez-Ortiz, J.R. González-Velasco, AIChE J. 49 (2003) 496–504.
[23] R. López-Fonseca, J.I. Gutiérrez-Ortiz, J.R. González-Velasco, Appl. Catal. A: Gen. 271 (2004) 39–46.
[24] K. Everaert, J. Baeyens, J. Hazard. Mater. B 109 (2004) 113–139.
[25] B. de Rivas, R. López-Fonseca, J.R. González-Velasco, J.I. Gutiérrez-Ortiz, J. Mol. Catal. A: Chem. 278 (2007) 181–188.
[26] I. Maupin, L. Pinard, J. Mijoin, P. Magnoux, J. Catal. 291 (2012) 104–109.
[27] S.D. Yim, I.S. Nam, J. Catal. 221 (2004) 601–611.
[28] J.-M. Giraudon, T.B. Nguyen, S. Siffert, J.-F. Lamonier, A. Aboukais, A. Vantomme, B.-L. Su, Catal. Today 137 (2008) 379–384.
[29] Y. Gu, Y. Yang, Y. Qiu, K. Sun, X. Xu, Catal. Commun. 12 (2010) 277–281.
[30] J.-F. Lamonier, T.B. Nguyen, M. Franco, S. Siffert, R. Cousin, Y. Li, X.Y. Yang, B.-L. Su, J.-M. Giraudon, Cata. Today 164 (2011) 566–570.
[31] L.Y. Jin, R.H. Ma, J.J. Lin, L. Meng, Y.J. Wang, M.F. Luo, Ind. Eng. Chem. Res. 50 (2011) 10878–10882.
[32] S. Pitkäaho, L. Matejova, S. Ojala, J. Gaalova, R.L. Keiski, Appl. Catal. B: Environ. 113–114 (2012) 150–159.
[33] S. Pitkäaho, T. Nevanperä, L. Matejova, S. Ojala, R.L. Keiski, Appl. Catal. B: Environ. 138–139 (2013) 33–42.
[34] K. Bahranowski, E.M. Serwicka-Bahranowska, T. Machej, A. Michalik, R. Janik, H. Piekarska-Sadowska, J. Janas, Polish Patent 199571 to ICSC PAS and AGH UST (2008).
[35] K. Bahranowski, E.M. Serwicka-Bahranowska, T. Machej, A. Michalik, R. Janik, H. Piekarska-Sadowska, J. Janas, Polish Patent 208217 to ICSC PAS and AGH UST (2011).
[36] E.M. Serwicka, K. Bahranowski, Catal. Today 90 (2004) 85–92.
[37] F. Figueras, Catal. Rev. 30 (1988) 457–499.
[38] J.T. Kloprogge, J. Porous Mater. 5 (1998) 5–41.
[39] A. Vaccari, Catal. Today 41 (1998) 53–71.
[40] S. Cheng, Catal. Today 49 (1999) 303–312.
[41] A. Gil, L.M. Gandia, M.A. Vicente, Catal. Rev. 42 (2000) 145–212.
[42] E.M. Serwicka, Pol. J. Chem. 75 (2001) 307–328.
[43] Z. Ding, J.T. Kloprogge, R.L. Frost, G.Q. Lu, H.Y. Zhu, J. Porous Mater. 8 (2001) 273–293.
[44] G. Centi, S. Perathoner, Micropor. Mesopor. Mater. 107 (2008) 3–15.
[45] A. Gil, S.A. Korili, R. Trujillano, M.A. Vicente, Pillared Clays and Related Catalysts, Springer, New York, 2010.
[46] L.C.A. Oliveira, R.M. Lago, J.D. Fabris, C. Solar, K. Sapag, Braz. J. Chem. Eng. 20 (2003) 45–50.
[47] P. Cafarelli, A. De Stefanis, G. Perez, A.A.G. Tomlinson, React. Kinet. Catal. Lett. 86 (2005) 163–169.
[48] L.C.A. Oliveira, R.M. Lago, J.D. Fabris, K. Sapag, Appl. Clay Sci. 39 (2008) 218–222.
[49] D. Li, C. Li, K. Suzuki, Appl. Clay Sci. 77–78 (2013) 56–60.
[50] T. Mishra, P. Mohapatra, K.M. Parida, Appl. Catal. B 79 (2008) 279–285.
[51] A. Aznárez, R. Delaigle, P. Eloy, E.M. Gaigneaux, S.A. Korili, A. Gil, Catal. Today (2014), http://dx.doi.org/10.1016/j.cattod.2014.07.024.
[52] K. Bahranowski, W. Włodarczyk, E. Wisła-Walsh, A. Gaweł, J. Matusik, A. Klimek, B. Gil, A. Michalik-Zym, R. Dula, R. Socha, E.M. Serwicka, Micropor. Mesopor. Mater. 202 (2015) 155–164.
[53] R. Lopez-Fonseca, J.I. Gutiérrez-Ortiz, M.A. Gutiérrez-Ortiz, J.R. González-Velasco, Catal. Today 107–108 (2005) 200–207.
[54] S. Yamanaka, G.W. Brindley, Clays Clay Miner. 27 (1979) 119–124.
[55] J. Sterte, Clays Clay Miner. 34 (1986) 658–664.
[56] A. Bernier, L.F. Admaiai, P. Grange, Appl. Catal. 77 (1991) 269–281.
[57] K. Bahranowski, A. Kielski, E.M. Serwicka, E. Wisła-Walsh, K. Wodnicka, Micropor. Mesopor. Mater. 41 (2000) 201–215.
[58] F. Rouquerol, J. Rouquerol, K. Sing, Adsorption by Powders & Porous Solids, Academic Press, London, 1999.
[59] E.P. Parry, J. Catal. 2 (1963) 371–379.
[60] H. Oguz, S. Koch, W. Weisweiler, Chem. Eng. Technol. 23 (2000) 395–400.
[61] M.L. Toebes, J.A. van Dillen, K.P. de Jong, J. Mol. Catal. A: Chem. 173 (2001) 75–98.
[62] N.B. Milić, Ž.D. Bugarčić, Transition Met. Chem. 9 (1984) 173–176.
[63] B.M. Weckhuysen, I.E. Wachs, R.A. Schoonheydt, Chem. Rev. 96 (1996) 3327–3349 (references therein).
[64] I.E. Wachs, Catal. Today 27 (1996) 437–455.
[65] J.R. McBride, K.C. Hass, W.H. Weber, Phys. Rev. B 10 (1991) 5016–5028.
[66] R. Bardhan, H.F. Zarick, A. Schwartzberg, C.L. Pint, J. Phys. Chem. C 117 (2013) 21558–21568.
[67] NIST X-ray Photoelectron Spectroscopy Database <http://srdata.nist.gov/xps/>.
[68] J.F. Moulder, W.F. Stickle, P.E. Sobol, K.D. Bomben, Handbook of X-ray Photoelectron Spectroscopy, PerkinElmer, Eden Prairie, MN, 1992.
[69] T.L. Barr, J. Phys. Chem. 62 (1978) 1801–1810.
[70] A. Hakuli, A. Kytökivi, A.O.I. Krause, Appl. Catal. A 190 (2000) 219–232.
[71] B. Liu, Y. Fang, M. Terano, J. Mol. Catal. A: Chem. 219 (2004) 165–173.
[72] D. Cordishi, M.C. Campa, V. Indovina, M. Occhiuzzi, J. Chem. Soc. Faraday Trans. 90 (1994) 207–212.
[73] B.M. Weckhuysen, R.A. Schoonheydt, F.E. Mabbs, D. Collison, J. Chem. Soc. Faraday Trans. 92 (1996) 2431–2436.
[74] A.L. Allred, J. Inorg. Nucl. Chem. 17 (1961) 215–221.
[75] T.L. Barr, J. Vac. Sci. Technol. A 9 (1991) 1793–1805.
[76] M.J. Guittet, J.P. Crocombette, M. Gautier-Soyer, Phys. Rev. B 63 (2001) 125117-1–125117-7.
[77] J. Valyon, I. Palinko, I. Kiricsi, React. Kinet. Catal. Lett. 58 (1996) 249–253.
[78] P.L. Hall, Clay Miner. 15 (1990) 321–335.
[79] W. Palczewska, Adv. Catal. 24 (1975) 245–291.
[80] M.W. Tew, J.T. Miller, J.A. van Bokhoven, J. Phys. Chem. C 113 (2009) 15140–15147.
[81] W.J. Shen, M. Okumura, Y. Matsumura, M. Haruta, Appl. Catal. A 213 (2001) 225–232.
[82] F. Li, Q. Zhang, Y. Wang, Appl. Catal. A 334 (2008) 217–226.
[83] R. Prins, Chem. Rev. 112 (2012) 2714–2738.
[84] B.M. Weckhuysen, R.A. Schoonheydt, J.M. Jehng, I.E. Wachs, S.J. Cho, R. Ryoo, S. Kijistra, E. Poels, J. Chem. Soc. Faraday Trans. 91 (1995) 3245–3253.
[85] A. Hakuli, M.E. Harlin, L.B. Backman, A.O.I. Krause, J. Catal. 184 (1999) 349–356.
[86] M.L. Zaki, N.E. Fouad, G.C. Bond, S.F. Tahir, Thermochim. Acta 285 (1996) 167–179.
[87] D.L. Hoang, H. Lieske, Thermochim. Acta 345 (2000) 93–99.
[88] E.P. Reddy, B. Sun, P.G. Smirniotis, J. Phys. Chem. B 108 (2004) 17198–17205.
[89] A. Amrute, C. Mondelli, J. Pérez-Ramírez, Catal. Sci. Technol. 2 (2012) 2057–2065.
[90] G.C. Bond, J.B.P. Tripathi, J. Chem. Soc. Faraday Trans. I 72 (1976) 933–941.
[91] H. Ming-Yuan, L. Zhonghui, M. Enze, Catal. Today 2 (1988) 321–338.
[92] M.R. Sun Kou, S. Mendioroz, M.I. Guijarro, Thermochim. Acta 323 (1998) 145–157.
[93] S.A. Bagshaw, R.P. Cooney, Chem. Mater. 5 (1993) 1101–1109.
[94] J.-F. Lambert, G. Poncelet, Top. Catal. 4 (1997) 43–56.
[95] A. Corma, H. Garcia, Chem. Rev. 103 (2003) 4307–4365.
[96] K. Ramanathan, J.J. Spivey, Combust. Sci. Technol. 63 (1989) 247–255.
[97] S.C. Petrosius, R.S. Drago, V. Young, G.C. Grunewald, J. Am. Chem. Soc. 115 (1993) 6131–6137.
[98] H.L. Greene, D.S. Prakash, K.V. Athota, Appl. Catal. B: Environ. 7 (1996) 213–224.
[99] R. Rachapudi, P.S. Chintawar, H.L. Greene, J. Catal. 185 (1999) 58–72.
[100] M.M.R. Feijen-Jeurissen, J.J. Jorna, B.E. Nieuwenhuys, G. Sinquin, C. Petit, J.P. Hindermann, Catal. Today 54 (1999) 65–79.
[101] A.M. Padilla, J. Corella, J.M. Toledo, Appl. Catal. B 22 (1999) 107–121.
[102] J. Janas, R. Janik, T. Machej, E.M. Serwicka, E. Bielańska, E. Bastardo-Gonzalez, W. Jones, Catal. Today 59 (2000) 241–248.
[103] S.D. Yim, K.H. Chang, D.J. Koh, I.S. Nam, Y.G. Kim, Catal. Today 63 (2000) 215–222.
[104] B. Miranda, E. Díaz, S. Ordóñez, A. Vega, F.V. Díez, M. Kang, C.H. Lee, Appl. Catal. A 266 (2004) 163–172.
[105] R. Ma, P. Hu, L. Jin, Y. Wang, J. Lu, Catal. Today 175 (2011) 598–602.
[106] T.R. Krawietz, P.W. Goguen, J.F. Haw, Catal. Lett. 42 (1996) 41–45.
[107] G. Sinquin, C. Petit, S. Libs, J.P. Hindermann, A. Kieneman, Appl. Catal. B 27 (2000) 105–115.
[108] L. Pinard, J. Mijoin, P. Magnoux, M. Guisnet, J. Catal. 215 (2003) 234–244.
[109] P. Mars, D.W. Van Krevelen, Chem. Eng. Sci. 3 (1954) 41–59 (special suppl.).
[110] L. Intriago, E. Diaz, S. Ordóñez, A. Vega, Micropor. Mesopor. Mater. 91 (2006) 161–169.
[111] W.A. Arnold, A.L. Roberts, Environ. Sci. Technol. 34 (2000) 1794–1805.
[112] S.K. Agarwal, J.J. Spivey, J.B. Butt, Appl. Catal. A 82 (1992) 259–275.